RhoA effectors LOK/SLK activate ERM proteins to locally inhibit RhoA and define apical morphology

Riasat Zaman[1,4], Andrew Lombardo[1,4], Cécile Sauvanet[1,2], Raghuvir Viswanatha[1,3], Valerie Awad[1], Locke Ezra-Ros Bonomo[1], David McDermitt[1] and Anthony Bretscher[1,5]

[1]Department of Molecular Biology and Genetics, Weill Institute for Cell and Molecular Biology, Cornell University, Ithaca, NY 14853

[2] Present Address: Unit of Structural Studies of Macromolecular Machines in Cellula, Department of Structural Biology and Chemistry, Institut Pasteur, CNRS UMR3528, Paris, France

[3] Present Address: Blavatnik Institute of Genetics, Harvard Medical School, 25 Shattuck St., Boston MA 02115

[4] These authors contributed equally to this work

[5] Address for correspondence: apb5@cornell.edu (A.B.)

Abstract

Activated Ezrin-Radixin-Moesin (ERM) proteins link the plasma membrane to the actin cytoskeleton to generate apical structures, including microvilli. Among many kinases implicated in ERM activation are the homologs LOK and SLK. CRISPR/Cas9 was used to knockout all ERM proteins or LOK/SLK in human cells. LOK/SLK knockout eliminates all ERM activating phosphorylation. The apical domain of cells lacking LOK/SLK or ERMs is strikingly similar and selectively altered, with loss of microvill, and junctional actin replaced by ectopic myosin-II containing apical stress-fiber-like structures. Constitutively active ezrin can reverse the phenotypes of either ERMs or LOK/SLK knockouts, showing that the major function of LOK/SLK is to activate ERMs. Both knockout lines have elevated active RhoA with concomitant enhanced myosin light chain phosphorylation, revealing that active ERMs are negative regulators of RhoA. As RhoA-GTP activates LOK/SLK to activate ERM proteins, the ability of active ERMs to negatively regulate RhoA-GTP represents a novel local feedback loop necessary for the proper apical morphology of epithelial cells.

Introduction

Essentially all eukaryotic cells are polarized, or have the potential to become polarized. This requires local regulation to define the morphology and composition of each cellular domain. A particularly well studied example is the intestinal epithelial cell with a highly ordered apical domain displaying abundant microvilli and having a protein and lipid composition distinct from the more planar basolateral membrane. While much is known about extrinsic cues that instruct the cell to polarize (Rodriguez-Boulan and Macara, 2014), much less is known about how the morphology of the individual domains is regulated. To address this, we have studied how the apical domain of epithelial cells is regulated to assemble bundles of actin filaments that support the plasma membrane of microvilli, in contrast to the flatter structure of the basolateral membrane.

The structural integrity of apical microvilli requires active ezrin/radixin/moesin (ERM) proteins (Fehon et al., 2010). These proteins exist in a cytoplasmic closed state and an active open conformation where the N-terminal FERM domain binds the plasma membrane and the C-terminal F-actin binding domain binds the underlying actin filaments (Gary and Bretscher, 1995). Activation requires phosphorylation of a conserved threonine, T567 in ezrin (Hayashi et al.,

1999; Matsui et al., 1998). The physiologically relevant kinase(s) responsible for ERM phosphorylation have been investigated for decades. Among the many kinases suggested are Rho kinase (Haas et al., 2007; Matsui et al., 1998; Tran Quang, 2000), PKCα (Ng et al., 2001); PKCθ (Pietromonaco et al., 1998), MST4 (Gloerich et al., 2012; ten Klooster et al., 2009), NcK-interacting kinase (Baumgartner et al., 2006) and LOK (Belkina et al., 2009; Viswanatha et al., 2012). More recent evidence has suggested that the related LOK and SLK are significant vertebrate kinases for ERM phosphorylation (Viswanatha et al., 2012), being the homologs of Slik that is responsible for phosphorylating the single ERM in flies, moesin (Hipfner et al., 2004). LOK and SLK belong to the germinal center-like kinase (GCK) -V subfamily of kinases (Kuramochi et al., 1997). They consist of a conserved N-terminal kinase domain, a less-conserved intermediate region and a moderately conserved C-terminal domain. The LOK C-terminal domain inhibits the kinase activity of LOK in cells, most likely through a cis-interaction, as well as targeting LOK to the apical membrane (Pelaseyed et al., 2017; Viswanatha et al., 2012). To maintain a strictly apical distribution, ezrin has to undergo phosphorylation/dephosphorylation cycles in which it is locally phosphorylated and subject to dephosphorylation by delocalized phosphatase Mypt1/PP1. As a result, constitutively active ezrin is unable to maintain apical restriction (Viswanatha et al., 2012).

The Rho family of small GTP-binding proteins are major regulators of microfilaments (Hall and Nobes, 2000). In early work Speck et al. (Speck et al., 2003) found that defects in fly moesin could be counteracted by antagonizing Rho activity, suggesting that ERM proteins might be able to regulate contractility in some manner. RhoA is capable of binding to a diverse range of effectors that influence the reorganization of actin into stress fibers and focal adhesions (Hall, 1998). Among these, the effector ROCK modulates microfilament organization and function in at least two distinct ways. First, it activates myosin II by directly phosphorylating the myosin regulatory light chain (Kimura et al., 1996) and inactivating myosin light chain phosphatase (Mypt1/PP1) (Kimura et al., 1996). Second, ROCK stabilizes F-actin by phosphorylating LIM kinase to abrogate its inhibitory activity towards cofilin, an F-actin destabilizing factor (Arber et al., 1998; Maekawa et al., 2017; Yang et al., 1998). The net effect results in an increase of cortical tension that can drive cellular contraction. ERM proteins have long been suggested to be downstream targets of ROCK, first as direct targets and then as indirect targets through Rho activation of PI-4-P5K (Matsui et al., 1999).

Until very recently, the potential relationship between Rho and LOK and SLK had not been studied. A BioID screen for regulators and effectors of RhoA in cultured cells identified SLK (and LOK) as effectors of RhoA (Bagci et al., 2020). RhoA-GTP was shown to bind to the C-terminal domain of SLK, the corresponding domain that negatively regulates the kinase activity and targets LOK to the apical domain. Moreover, active RhoA can activate SLK in its ability to phosphorylate ezrin. Thus, a direct pathway exists from RhoA-GTP to its effector LOK/SLK to ERM protein activation.

Further uncovering the functions and exploring signaling pathways related to ERM proteins and LOK and SLK in cultured cells has been hampered by redundancy, and the possibility that they perform essential functions. Here we show that it is possible to generate cultured cells lacking all ERM proteins, and cells lacking both LOK and SLK. This has allowed us to explore the roles of these proteins, both by characterizing cells lacking them, but also by re-introduction of variants. Surprisingly, cells lacking LOK and SLK have a strikingly similar phenotype to cells lacking ERM proteins. Our results establish that LOK and SLK are the major, and possibly only, kinases that phosphorylate the conserved threonine of ERM proteins in epithelial cells. Further, rescue experiments indicate that ERM proteins are the major substrates of LOK and SLK that regulate cell morphology. Moreover, loss of either LOK/SLK or ERM proteins selectively modifies the apical actin cytoskeleton of epithelial cells by elevating RhoA signaling to redistribute actin from microvilli and junctions to generate ectopic apical stress fibers. We propose that LOK/SLK and ERM proteins function as a module that defines apical morphology of epithelial cells in a process that involves a negative feed-back loop to locally down-regulate Rho activity.

Results

Jeg3 cells lacking ERM proteins or LOK/SLK are viable and lack microvilli

In earlier studies we described human cells modified by CRISPR/Cas9 to lack expression of LOK (Pelaseyed et al., 2017), but so far no cultured cells have been described that genetically lack specific ERM proteins. We set out to determine if cells lacking all ERM proteins, or lacking both LOK and SLK, are viable, and if so, what phenotypes were conferred. Our studies were performed in Jeg3 epithelial cells derived from a human choriocarcinoma as these cells exhibit

102 abundant apical microvilli (Pakkanen et al., 1987). Of the ERM proteins, Jeg3 cells express
103 ezrin and radixin, but not moesin (Figure 1A). We first used CRISPR/Cas9 to isolate cells
104 lacking either ezrin or radixin or SLK (Figure 1A). We then generated pairs of double knockout
105 cells, lacking all detectable ezrin and radixin, or LOK and SLK (Figure 1A). Importantly, moesin
106 was not expressed in the Jeg3 ezrin$^{-/-}$ radixin$^{-/-}$ cells—which can be identified as moesin is
107 expressed in HeLa cells (Figure 1A, lane 1). Thus, the Jeg3 cells lacking all ERM proteins are
108 viable. Likewise, Jeg3 cells lacking both LOK and SLK are viable. However, both ezrin$^{-/-}$ radixin$^{-/-}$
109 and LOK$^{-/-}$ SLK$^{-/-}$ cells grew slower than their wildtype counterparts (Figure S1A).
110
111 As ERM proteins and LOK and SLK have been implicated in the formation of microvilli
112 on these cells, we examined whether single and double knockout cells retained microvilli. To
113 assess the presence of microvilli, we could not use the traditional ERM proteins as markers, so
114 we utilized labelled wheat germ agglutinin (WGA) that binds to plasma membrane glycoproteins
115 and allows for the identification of cell surface structures. In wildtype cells, WGA colocalizes with
116 ezrin in surface microvilli (Figure 1B). Consistent with earlier reports, individual reduction of
117 ezrin or genetic loss of LOK resulted in a reduction in the number of cells with apical microvilli,
118 whereas loss of radixin or SLK had little phenotype (Figure 1C, Figure S1B). Strikingly ezrin$^{-/-}$
119 radixin$^{-/-}$ and LOK$^{-/-}$ SLK$^{-/-}$ cells totally lack microvilli, with WGA staining mostly associated with
120 membrane ruffles that form above membrane contact sites (Figure 1B, arrows and 1C). Ezrin is
121 cytosolic in LOK$^{-/-}$ SLK$^{-/-}$ cells, consistent with phosphorylation by LOK/SLK being required to
122 activate it. Stable expression of ezrin in ezrin$^{-/-}$ radixin$^{-/-}$ cells and LOK in LOK$^{-/-}$/SLK$^{-/-}$ restored
123 the presence of microvilli to the cell surface. We conclude that both an ERM protein and LOK or
124 SLK are necessary for the presence of apical microvilli. We also examined the localization of the
125 interactor of active ezrin, EBP50 (ERM-binding phosphoprotein of 50kD)/NHERF1 (Figure 1D).
126 Whereas EBP50 was present in microvilli in wildtype cells, in both double knockout cell lines
127 EBP50 was cytosolic. Both the WGA and EBP50 staining supports the conclusion that the loss
128 of ERMs or LOK/SLK disrupts the presence of microvilli from the apical surface.
129
130 **LOK/SLK are the major kinases for ERM phosphorylation**
131
132 ERM proteins undergo activation by C-terminal phosphorylation to exhibit their
133 membrane-cytoskeletal linking function (Pearson et al., 2000; Turunen et al., 1994). The identity
134 of the relevant kinase has been controversial, so we assessed the contribution of LOK and SLK
135 to ERM phosphorylation in LOK$^{-/-}$ SLK$^{-/-}$ cells. Using an antibody that detects the relevant

136 epitope on all ERM proteins (phosphorylation of T567 in ezrin, T564 in radixin, and T558 in
137 moesin) we found that LOK$^{-/-}$ SLK$^{-/-}$ cells appeared to be entirely devoid of all ERM
138 phosphorylation (Figure 2A). However, because the pERM antibody produces a small
139 background staining to unphosphorylated ezrin (Pelaseyed et al., 2017), we repeated the
140 experiment employing phos-Tag gels in which phosphorylated ERMs migrate slower than their
141 unphosphorylated counterparts. Again, we were unable to detect any phosphorylated ERM
142 proteins in the absence of LOK and SLK (Figure 2B), so LOK and SLK appear to be the only
143 significant ERM kinases in Jeg3 cells.
144
145 To explore if this is true in other cells, we also generated LOK$^{-/-}$ SLK$^{-/-}$ knockouts in HeLa
146 cells. While these cells survived clonal isolation and lysate collection, they grew very slowly and
147 could not be maintained. Nevertheless, analysis of cell lysates revealed that in HeLa cells as
148 well, LOK and SLK are the major ERM kinases (Figure 2A). Further, we also tried to knock out
149 LOK and SLK in epithelial Caco-2 cells, which proved inviable past clonal selection indicating
150 the importance of these kinases. Likewise, we tried to isolate HeLa and Caco-2 cells lacking
151 ezrin. Although we nursed the growth of enough cells to demonstrate loss of ezrin, they could
152 not be passaged. These results suggest that ERM proteins are more important for viability in
153 HeLa and Caco-2 cells than in Jeg-3 cells. It was fortuitous that we started with Jeg-3 cells as it
154 has allowed us to use the double knock-outs to explore in more detail the phenotypes conferred
155 by loss of these proteins, or reintroduction of variants.
156
157 In transfection-based experiments, expression of LOK-GFP-Flag was able to both
158 restore ERM phosphorylation and apical microvilli to LOK$^{-/-}$ SLK$^{-/-}$ cells (Figures 1B&C, 2D).
159 LOK contains an N-terminal kinase domain and C-terminal domain responsible for both
160 regulating and localizing the kinase (Pelaseyed et al., 2017). As expected, expression of a
161 K65R kinase-inactive variant of LOK was unable to restore phosphorylation or microvilli (Figure
162 2C,D).
163
164 **Absence of activated ERM proteins induces the formation of apical actin/myosin II**
165 **bundles and alters cell-cell junctions of epithelial cells**
166
167 To explore what additional phenotypes might be associated with loss of ERM proteins
168 and their activating kinases, we examined the structure of cell junctions and the actin
169 distribution in the knockout cells. A characteristic feature of epithelial cells is their ability to form

170 strong cell-to-cell contact sites. Using the tight junction marker ZO-1, we observe a remarkably
171 similar phenotype in ezrin$^{-/-}$ radixin$^{-/-}$ and LOK$^{-/-}$ SLK$^{-/-}$ cells. In both cases, the cells maintain cell-
172 to-cell contacts, but the contact sites are uneven and occasionally have breaks in their ZO-1
173 and greatly reduced junctional actin staining (Figure 3A, magenta arrows). In contrast, wildtype
174 Jeg3 cells form uniform and relatively linear contacts along cell junctions co-staining with actin
175 (Figure 3A, blue arrows). By determining the ratio between the contour length and shortest
176 distance in ZO-1 staining from a three-cell junction to the next, we quantified the straightness of
177 the tight junctions in cells under various conditions (Figure 3B). This measurement of tortuosity
178 was slightly above 1.0 for wildtype cells, reflecting their almost linear nature. For either ezrin$^{-/-}$ or
179 LOK $^{-/-}$ this rose to 1.15, and for ezrin$^{-/-}$ radixin$^{-/-}$ and LOK$^{-/-}$/SLK$^{-/-}$ cells to about 1.2, indicating
180 greater distortion/waviness of the interface. As with loss of microvilli, loss of just ezrin or LOK is
181 more severe than loss of just radixin or SLK, and both double mutants exhibit the most severe
182 phenotype. This tortuosity of the junctions was rescued by expressing ezrin in the ezrin$^{-/-}$ radixin^{-}
183 $^{/-}$ cells and LOK in the LOK$^{-/-}$ SLK$^{-/-}$ cells (Figure 3A).
184
185 We also noticed an additional striking effect on the actin distribution in which significantly
186 more F-actin is seen spanning the apical domain in the double knockout cells compared to their
187 wild type counterpart. Therefore, we examined the F-actin distribution in the basal and apical
188 regions of the cells. ZO-1 localization is found near the apical region of both wildtype and
189 knockout cells, so we split confocal planes into those containing ZO-1 staining and above (the
190 apical domain), and those below ZO-1 staining (the basolateral domain). Whereas the wildtype
191 cells display actin in microvilli and along the cell junctions, both ezrin$^{-/-}$ radixin$^{-/-}$ and LOK$^{-/-}$/SLK$^{-/-}$
192 cells were noticeably different with actin bundles extending across the apical domain that
193 correlate with the uneven contour of the tight junctions (Figure 3A). In contrast, there is no
194 apparent difference in the basal actin network between the cells (Figure 3A), which is
195 underscored by the similarity of focal contacts at the basal surfaces (Figure S2A). We quantified
196 this difference by measuring the ratio of the actin intensity at the apical versus the basal side of
197 the cells (Figure 3C). Both KO cells were found to have an increase in the density of actin found
198 exclusively at the apical surface compared to wildtype cells (Figure 3A and C). The aberrant
199 apical actin bundles are rescued by introduction of ezrin into ezrin$^{-/-}$ radixin$^{-/-}$ and of LOK into
200 LOK$^{-/-}$/SLK$^{-/-}$ cells (Figure 3 A-C).
201
202 The apical actin structures seen in ezrin$^{-/-}$ radixin$^{-/-}$ and LOK$^{-/-}$ SLK$^{-/-}$ cells contained
203 bundles, similar in appearance to stress fibers. The expression level of the stress fiber marker α

204 -actinin and focal adhesion marker vinculin were unchanged in the knockout cells (Figure S3).
205 We next explored if these bundles could have contractile properties by staining for non-muscle
206 myosin-IIB (myo-IIB). While striated bundles of myo-IIB and actin were not completely absent in
207 the apical region of wildtype cells, a stronger intensity and more frequent clusters of myo-IIB
208 was observed in ezrin$^{-/-}$ radixin$^{-/-}$ cells (Figure 4A, arrows). This phenotype was also seen and
209 enhanced in LOK$^{-/-}$SLK$^{-/-}$ cells where the entire apical domain appeared covered in myo-IIB
210 puncta and actin filaments. Using deconvolution microscopy, we could see characteristic
211 myosin-II sarcomeric-like striations indicative of a contractile structure (Figure 4B). Together our
212 results show that lack of activated ERMs, either due to loss of the proteins or their activating
213 kinases, selectively redistributes actin in the apical domain into contractile bundles.
214
215 **Enhanced actin assembly in the apical domain is responsible for the junctional defects of**
216 **knockout cells**
217
218 In wildtype cells, apical actin in the microvilli treadmills continuously resulting in turnover
219 in the ~2-10 min time-frame (Loomis et al., 2003; Meenderink et al., 2019). We investigated the
220 possibility that the abnormal actin bundles seen in knockout cells might arise in part from
221 reduced actin turnover in the apical domain. To test this, we treated wildtype cells with the actin
222 stabilizing drug Jasplakinolide to reduce actin turnover. Remarkably, treatment of wildtype cells
223 with 500nM Jasplakinolide for 30 minutes induced both the formation of actin bundles in the
224 apical domain and increased the tortuosity of the tight junctions (Figure 5A and B, lanes 1 and
225 2) in a manner closely resembling the phenotype of ezrin$^{-/-}$ radixin$^{-/-}$ or LOK$^{-/-}$ SLK$^{-/-}$ cells (Figure
226 3A). The addition of Jasplakinolide in all three cell lines further increased the abundance of
227 apical F-actin networks across each cell, correlating with the increased tight junction tortuosity
228 and breaks between neighboring cells (Figure 5A, magenta arrows and C).
229
230 If enhanced actin assembly in the double knockout cells is responsible for the observed
231 tortuosity of the junctions, increasing depolymerization in these cells might rescue this
232 phenotype. Upon treatment of either of the double-knockout cells with the actin-depolymerizing
233 drug Latrunculin B or actin plus-end-capping drug Cytochalasin D, tight junction tortuosity ratios
234 in the knockout cells were restored to levels comparable to wildtype cells (Figure 5A, B and
235 S5A). Interestingly, Latrunculin B treatment of cells did not completely restore the balance of F-
236 actin between the apical and basolateral domains to wild type levels (Figure 5C). Analysis of the
237 apical/basolateral actin distribution after these drug treatments was complicated by the finding

238 that apical actin appears to be more resistant to disassembly by Latrunculin B than its
239 basolateral counterpart (Figure S5B). Nonetheless, in contrast to Jasplakinolide-treated cells,
240 Latrunculin B treatment results in reorganization of actin towards junctions Figure 5A, blue
241 arrows) and relief of junctional defects (Figure 5B). Meanwhile, stabilization by Jasplakinolide
242 redistributes actin away from the junctions and across the cell promoting junctional defects
243 (Figure 5A and B). In summary, our data shows ezrin$^{-/-}$ radixin$^{-/-}$ and LOK$^{-/-}$ SLK$^{-/-}$ cells become
244 more similar to wildtype when treated with Latrunculin B, while wildtype cells become more like
245 the knockout cells when treated with Jasplakinolide. Therefore in the absence of active ERMs,
246 excessive actin assembly generates contractile bundles that provide forces perpendicular to
247 junctions.
248
249 To assess how the actin redistribution might affect the mechanics of the apical surface,
250 we utilized Atomic Force Microscopy (AFM) to measure their stiffness. Cells were allowed to
251 grow to a confluent monolayer and then indented to a maximum force of 1nN (Figure 5D inset).
252 The resulting force vs. distance curves were then used to identify the initial AFM probe tip
253 contact point, allowing us to fit to a hertz equation to calculate the Young's modulus (E) stiffness
254 parameter (Huth, Sindt, & Selhuber-Unkel, 2019). Indentations from each condition were then
255 averaged to produce a mean curve for wild type, ezrin$^{-/-}$ radixin$^{-/-}$ and LOK$^{-/-}$ SLK$^{-/-}$ cells (Figure
256 5D). Of the 1,091 total force indentations preformed, both LOK$^{-/-}$ SLK$^{-/-}$ (E = 260±45 kPa
257 Median±) and ezrin$^{-/-}$ radixin$^{-/-}$ (E = 166±52 kPa) cells are significantly stiffer then WT cells (E =
258 117±65 kPa) (Figure 5E). The finding that LOK$^{-/-}$SLK$^{-/-}$ cells are more rigid than ezrin$^{-/-}$ radixin$^{-/-}$
259 cells is consistent with the enhanced levels of stress-fiber-like bundles seen in the apical
260 domain of LOK$^{-/-}$SLK$^{-/-}$ cells described in Figure 4. Together these results indicate that activated
261 ERM proteins suppress the formation of apical actin bundles to affect the mechanical properties
262 of the apical domain.
263
264 **Activated ezrin Rescues both ezrin$^{-/-}$ radixin$^{-/-}$ and LOK$^{-/-}$SLK$^{-/-}$ cells**
265
266 The phenotypic similarity of the ezrin$^{-/-}$ radixin$^{-/-}$ and LOK$^{-/-}$ SLK$^{-/-}$ cells, suggested that
267 essentially all the phenotypes of LOK$^{-/-}$ SLK$^{-/-}$ cells are due to the lack of ERM phosphorylation.
268 If this is the case, introduction of mutationally activated ezrin in either of the double knockout
269 cells should rescue them in a similar manner. We therefore introduced the constitutively active
270 phosphomimetic ezrin-T567D mutant into both ezrin$^{-/-}$ radixin$^{-/-}$ and LOK$^{-/-}$/SLK$^{-/-}$ cells.
271 Remarkably, phosphomimetic ezrin suppressed both equally with restoration of microvilli (Figure

272 6A). The rescue isn't perfect, as constitutively active ezrin is seen both apically and basolaterally
273 because restriction to the apical domain requires ezrin phosphocycling (Viswanatha et al.,
274 2012). Expression of constitutively active phosphomimetic ezrin-T567D is also able to suppress
275 tight junction defects and the excess apical actin bundles seen in knockout cells implying that
276 active ezrin can regulate actin at the cortex (Figure 6B-D). These results suggest that the
277 primary role for LOK and SLK in Jeg3 cells is to phosphorylate ERMs.
278
279 **Phosphorylated ERM proteins regulate myosin-II activity through RhoA Activation**
280
281 The appearance of apical stress-fiber-like cables in cells lacking activated ERMs is
282 suggestive of local enhanced RhoA activity. Rho-associated kinase (ROCK) is a major effector
283 of RhoA-GTP that can activate myosin-II by directly phosphorylating myosin light chain 2
284 (MLC2), and this is counteracted by the phosphatase PP1 utilizing the Mypt1 subunit. Total non-
285 muscle myosin-II expression showed no differences between wild type and LOK$^{-/-}$SLK$^{-/-}$ or ezrin^{-}
286 $^{/-}$ radixin$^{-/-}$ cells (Figure S2B). The level of endogenous MLC2 phosphorylation was found to be
287 very low in wildtype cells and 3-4 fold enhanced in both ezrin$^{-/-}$ radixin$^{-/-}$ and LOK$^{-/-}$SLK$^{-/-}$ cells
288 (Figure 7A and B). To increase the level of phosphorylation, we treated cells briefly with
289 calyculin A that inhibits the phosphatase PP1. Treatment of wildtype cells with calyculin A
290 enhanced the level of MLC2 phosphorylation, and greatly enhanced the level seen in both of the
291 knockout lines. These results reveal that activated ERM proteins negatively regulate
292 phosphorylation of MLC2 and hence myosin-II activation.
293
294 MLC2 phosphorylation is either mediated by ROCK, or via Ca^{2+}-calmodulin-dependent
295 myosin light chain kinase. To explore which pathway is involved, we treated wildtype and double
296 knockout cells with the specific ROCK inhibitor Y-27632. This resulted in equalization of
297 phospho-MLC2 levels (Figure 7C), indicating that the enhanced level of phospho-MLC2 seen in
298 knockout cells is upstream of ROCK. We therefore measured the level of endogenous RhoA-
299 GTP by passing total cell lysates over Rhotekin-GST beads and measuring the relative levels of
300 RhoA retained. Both ezrin$^{-/-}$ radixin$^{-/-}$ and LOK$^{-/-}$SLK$^{-/-}$ cells were found to have about a 3-fold
301 higher level of active RhoA than wildtype cells (Figure 7D). In addition to regulating MLC2
302 phosphorylation, ROCK also regulates actin dynamics through the LIM kinase-cofilin pathway
303 (Arber et al., 1998; Maekawa et al., 2017; Yang et al., 1998), which may explain in part the
304 altered actin dynamics discussed earlier.
305

306 A recent report showed that active RhoA binds directly to the C-terminal domain of SLK
307 and this promotes its dimerization and ability to phosphorylate ERM proteins (Bagci et al.,
308 2020). In earlier work we showed that expression of the C-terminal region of LOK (LOK_310-
309 968-GFP-Flag or LOK-CTD-GFP-Flag) acts as a potent dominant negative to strongly inhibit
310 phosphorylation of ERM proteins (Viswanatha et al., 2012). To explore if this region of LOK
311 binds to RhoA, we expressed LOK-CTD-GFP-Flag either alone or with constitutively active HA-
312 RhoA-L30 and immunoprecipitated with Flag antibodies in WT Jeg3 cells (Figure 7E). RhoA
313 was recovered in the Flag immunoprecipitates, indicating an interaction between the two.
314 Therefore, both LOK and SLK are effectors of RhoA.
315
316 Collectively these results suggest a model in which RhoA selectively regulates the apical
317 domain of epithelial cells in a negative feedback loop involving active ERM proteins (Figure 7F).
318 RhoA activates both the kinases LOK/SLK and ROCK to mediate phosphorylation of ERM
319 proteins and MLC2, respectively. ROCK also negatively regulates PP1, the phosphatase that
320 dephosphorylates both pMLC and pERMs. Phosphorylated ERMs localized exclusively in the
321 apical domain regulate RhoA in a negative feedback loop.
322
323 **Phosphorylated ERMs negatively regulate myosin contractility**
324
325 If the model presented in Figure 7F is valid, a prediction is that a functional difference in
326 contractile force production should exist between wildtype and knockout cells. It is known that
327 cultured cells treated with calyculin A to elevate the level of myosin-II activity will ultimately
328 contract (Ishihara et al., 1989). Therefore, we examined the contraction of spread LOK$^{-/-}$SLK$^{-/-}$
329 and ezrin$^{-/-}$radixin$^{-/-}$ cells compared with wildtype cells in the presence of 10nM Calyculin A over
330 the course of 1 hour. Under this treatment a small fraction of WT cells showed rounding and
331 detachment from the plate. In a dramatic difference, LOK$^{-/-}$SLK$^{-/-}$ and ezrin$^{-/-}$radixin$^{-/-}$ cells
332 showed significant rounding and detachment from neighboring cells in under 30 minutes (Figure
333 8A, Movie S1). We confirmed that the contractility is a result of enhanced myosin-II activity as
334 the calyculin A induced contraction was prevented by inclusion of the myosin-II inhibitor
335 blebbistatin, which showed no rounding or contraction in any cell type after 1 hour (Figure 8B,
336 Movie S2). These results are in agreement with Figure 7A showing an increased level of MLC
337 phosphorylation in the knockout cells in the presence of calyculin A. However, calyculin A also
338 results in enhanced phosphorylation of ERMs (Viswanatha et al., 2012), so we wished to
339 examine if the contractility difference induced by calyculin A was present in cells where the level

340 of active ezrin was unchanged. To achieve this, we stably expressed the active phosphomimetic
341 ezrin-T567E in double knockout cells. Under these conditions both LOK$^{-/-}$ SLK$^{-/-}$ and ezrin$^{-/-}$
342 radixin$^{-/-}$ cells expressing ezrin-T567E the contraction induced by calyculin A was greatly
343 reduced (Figure 8B, Movie S3). This implies that it is the loss of active ERMs, and not the loss
344 of LOK and SLK independent of ERMs, that regulates the contractility due to enhanced RhoA-
345 GTP.
346
347
348 **Discussion**
349
350 In this study we have investigated the phenotypes conferred by loss of ERM proteins, or
351 their activators, LOK and SLK. In some cells loss of LOK and SLK, or in fact just ezrin in HeLa
352 or Caco-2 cells, are too unhealthy to maintain, indicating that ERM proteins and their activating
353 kinases can be almost essential. This is consistent with the situation in mice, flies and the
354 nematode worm, where loss of ezrin or the single ERM protein (flies and worm), is lethal
355 (Jankovics et al., 2002; Saotome et al., 2004). Additionally, the loss of SLK in mouse or the
356 single homolog Slik in the fly is also lethal (Hipfner and Cohen, 2003). Loss of just LOK in the
357 mouse has a more modest phenotype (Belkina et al., 2009), presumably due to partial
358 compensation by SLK. We were fortunate to start with a cell line, Jeg-3, that can tolerate loss of
359 either all ERM proteins, or both LOK and SLK, as this allowed us to study their phenotypes. As
360 far as we are aware, these are the first vertebrate cells isolated genetically lacking either all
361 ERM proteins or the kinases LOK and SLK.
362
363 Previous studies have shown that wildtype epithelial cells maintain ~50% of their ezrin in
364 the active, phosphorylated state with cycling between active and inactive states occurring on the
365 scale of ~2 minutes (Viswanatha et al., 2012). Proper preservation of this balanced system is
366 critical for maintaining a polarized morphology (Viswanatha et al., 2012) and is consistent with
367 mislocalization, overexpression, and hyper-phosphorylation of ezrin found in types of human
368 cancers (reviewed in Clucas and Valderrama, 2015). Our finding that loss of LOK and SLK
369 results in ablation of all detectable ezrin-T567 phosphorylation is consistent with LOK and SLK
370 being the major, if not only, kinases that can phosphoryate the ERM regulatory threonine (T567
371 in ezrin). This result is in agreement with earlier descriptions that Slik is solely responsible for
372 the activation of fly moesin (Hipfner et al., 2004).
373

374 A remarkable aspect of our results is that cells lacking either all ERM proteins or LOK
375 and SLK are phenotypically very similar. Both grow slower, have lost all apical microvilli, have
376 greatly reduced junctional actin but also an aberrantly high level of apical F-actin and myosin,
377 have wavy cell junctions, have a stiffer apical domain, contract abnormally in the presence of
378 the phosphatase calyculin A, and both have elevated levels of Rho-GTP. This raises the
379 question whether the ERM proteins are the sole substrate of LOK/SLK. An intricate multi-step
380 mechanism is involved in phosphorylation of ezrin by LOK. In outline, it requires priming of ezrin
381 by PIP_2, then insertion of the C-terminal region of LOK between the ezrin FERM and C-terminal
382 F-actin binding domain, which gives access for the kinase domain to bind a recognition site and
383 ultimately phosphorylate T567 (Pelaseyed et al., 2017). This mechanism, together with the
384 strong preference for a tyrosine two residues upstream of the targeted threonine (Belkina et al.,
385 2009), makes phosphorylation of ERM proteins highly selective. This elaborate coincidence
386 detection mechanism involved in LOK phosphorylation of ezrin coupled with the ability of
387 mutationally active ezrin (ezrin-T567D) to suppress the phenotype of LOK/SLK cells strongly
388 supports the notion that ERM proteins are the major functional substrates. Using a phospho-
389 proteomics approach in unpublished work, we sought to identify additional LOK/SLK substrates.
390 While we encountered many phosphopeptides whose level was elevated in wild type cells
391 compared with LOK/SLK knockout cells, none had the appropriate LOK/SLK consensus
392 sequence. Therefore, LOK/SLK and ERM proteins appear to work together as a functional unit.
393 Although we were not able to identify additional LOK/SLK substrates, technical limitations may
394 have obscured them from our analysis. In support of this possibility, the phenotypes of LOK/SLK
395 cells enumerated above were almost always more severe than in the ERM knockout cells. Thus,
396 the possibility remains that there is another minor substrate, functionally redundant with ERM
397 proteins, cannot be ruled out.
398
399 While we expected to see loss of microvilli in cells lacking ERM proteins, we were
400 surprised to encounter an extensive actin/myosin-II network in the apical domain replacing the
401 junctional and microvillar actin. This phenotype was also seen in LOK/SLK knockout cells,
402 implying that active ERM proteins can regulate the myosin and actin distribution in the apical
403 domain. RhoA-GTP is known to positively regulate non-muscle myosin-II activity through
404 ROCK1 as well as F-actin turnover through LIM kinase and cofilin. Since both actin turnover and
405 myosin contractility are altered in the absence of pERMs, we then considered a possible over-
406 activation of RhoA in the knockout cells. Indeed, the level of RhoA-GTP was significantly

407 elevated in both ERM and LOK/SLK knockout cells. Thus, active ERMs are negative regulators
408 of RhoA (Figure 7F).
409
410 There have been several indications of a connection between ERM protein function and
411 RhoA. First, ROCK1 was reported as the kinase that phosphorylates ERM proteins, in part
412 because ROCK1 over expression resulted in formation of microvilli in cos-7 cells and its
413 reported ability to phosphorylate radixin *in vitro* (Matsui et al., 1998; Oshiro et al., 1998). With
414 the finding that Mypt1/PP1 is the phosphatase responsible for dephosphorylating ERM proteins
415 (Fukata et al., 1998), and that Mypt1/PP1 is negatively regulated by ROCK1 (Velasco et al.,
416 2002), the earlier result can be explained. In a genetic study in the fly, phenotypes resulting
417 from loss of moesin can be rescued by also reducing the level of RhoA (Speck et al., 2003).
418 Recent work has shown that RhoA-GTP directly dimerizes and activates SLK (Bagci et al.,
419 2020). As phosphorylated ERM proteins act as negative regulators of RhoA-GTP, a local
420 feedback cycle exists in which RhoA-GTP and pERMs regulate each other's activity specifically
421 across the apical domain (Figure 7F).
422
423 RhoA is a well recognized spatial regulator of the adherens junctions between epithelial
424 cells (reviewed in Hartsock and Nelson, 2008; Marjoram et al., 2014; McCormack et al., 2013).
425 Active RhoA is highly enriched at junctions through the action of various regulators, including
426 the RhoA-GEFs p114RhoGEF and ECT2, and indirectly through active myosin IIA recuitment of
427 ROCK1 to phosphorylate and inactivate the ability of Rnd3 to recruit p190B RhoA-GAP
428 (Ratheesh et al., 2012; Reyes et al., 2014; Terry et al., 2011). Misregulation of RhoA can affect
429 the mechanical tension between junctions of neighboring epithelial cells (Zihni et al., 2014).
430 Indeed, this is what we observe by knocking out active ERMs. As a consequence of removing
431 active ERMs, we find that F-actin bundles are re-distributed away from the junctions and into
432 actomyosin networks across the apical terminal web. This state can be mimicked in wildtype
433 epithelial cells by introducing an actin stabilizing drug like Jasplakinolide. Conversely, the actin
434 in knockout cells can be re-directed back towards junctions by adding actin depolymerizing drug
435 Latrunculin B. A similar phenomenon is seen when anillin is manipulated in epithelial cells,
436 where anillin knockdown cells produce low tensile forces and overexpression produced high
437 tensile forces due to misregulation of medial-apical F-actin (Arnold et al., 2019). Thus, local
438 spatial regulation of proteins like ERMs and anillin can influence the RhoA-dependent actin
439 turnover at the apical domain and junctions of epithelial cells. As LOK is an effector of active
440 RhoA and is located to the microvilli, and not the cell-cell junctions, a subpopulation of RhoA

441 must be specifically regulated at across the apical surface of epithelial cells. The activity of this
442 local RhoA subpopulation is negatively regulated by phosphorylated ERM proteins, presumably
443 through either a Rho-GEF or a Rho-GAP. In the fly RhoGAP Conundrum has been shown to
444 bind moesin and act as a negative regulator of Rho1. However, since deletion of Conundrum
445 has no obvious phenotype there is likely functional redundancy with another RhoGAP (Neisch et
446 al., 2013). Our future work will be aimed at identifying the factor(s) that allow active ERMs to
447 mediate local negative regulation of RhoA-GTP.

448 A more distant member of the ERM protein family is merlin, the product of the tumor
449 suppressor gene (*NF2*) in which defects result in Neurofibromatosis-II (Sanson et al., 1993;
450 Trofatter et al., 1993). Merlin has an N-terminal FERM domain and a negative regulatory C-
451 terminal. The FERM domain of merlin can bind the C-terminal domain of ERM proteins, and *vice*
452 *versa* (Bretscher et al., 2000). Considerable work suggests that ERM proteins and merlin act
453 antagonistically, especially in the organization of the plasma membrane during endocytosis
454 (Chiasson-Mackenzie et al., 2018; Hebert et al., 2012). It will be interesting to explore if active
455 merlin can regulate RhoA activity, or if merlin-deficient cells that fail to modulate the activity of
456 ERM proteins have a lower level of RhoA-GTP.

457 In summary, we have found that ERM proteins and their activators LOK/SLK function in
458 the same pathway as a unit to build microvilli on the apical surface of epithelial cells and locally
459 modulate the level of RhoA-GTP in a feedback inhibition cycle. The next challenge will be to
460 understand how this feedback loop is regulated and restricted to the apical domain.

461

462 **Materials and Methods**

463 **Reagents & cDNAs**

464 Ezrin antibodies were either a mouse anti-ezrin antibody (CPCT-ezrin-1 supernatant
465 concentrate obtained from the Developmental Studies Hybridoma) used at 1:1,250 (Western
466 blot) or 1:100 (immunofluorescence) or a previously characterized rabbit polyclonal antibody
467 raised against full-length human ezrin (Bretscher, 1989) and used at 1:1,000 (Western blot) or
468 1:200 (immunofluorescence). Rabbit anti-EBP50 was also a previously characterized antibody
469 (Reczek et al., 1997) and was used at 1:50 (immunofluorescence). Mouse anti-ZO1 (BD
470 Biosciences, Cat #610966) was used at 1:100 (immunofluorescence). Rabbit anti-radixin (Cell

471 Signaling, Cat #C4G7) used at 1:1000 (Western blot) to blot for both radixin (80kDa) and
472 moesin (75kDa). Rabbit anti-pERM (raised against re-combinant phosphopeptide) was used at
473 1:1000 (Western blot). Rabbit anti-LOK used at 1:500 (western blot) and rabbit anti-SLK used at
474 1:100 (Western blot) were purchased from Bethyl Laboratories, Inc. Mouse anti-Flag used at
475 1:5,000 (Western blot) and mouse anti-tubulin used at 1:5,000 (Western blot) were obtained
476 from Sigma-Aldrich. Mouse anti-GFP used at 1:100 (immunofluorescence) was obtained from
477 Santa Cruz Biotechnology, Inc. Rabbit antibodies for anti-myosin-light-chain-2 (Cat #3672) and
478 anti-phospho-myosin-light-chain-2 (raised against phospho-Thr18/Ser19; Cat #3674) were
479 purchased from Cell Signaling and used at 1:500 (Western blot). Monoclonal Mouse anti-RhoA
480 antibody (Cytoskeleton inc. Cat#ARH05) was obtained through the Cytoskeleton inc Rho A
481 activation Assay Biochem Kit and used at 1:500. Rabbit antibody for anti non-muscle-myosin-
482 IIB from (BioLegend, Cat. No. 909902) was used at 1:100 (Western blot and
483 immunofluorescence). Rabbit polyclonal antibodies raised by standard procedures against
484 Vinculin, brush boarder myosin-II and alpha-acitinin purified from chicken gizzard were used at
485 1:2000, 1:200 or 1:200 respectively for supplemental figure 1 western blotting. For actin
486 staining, alexa fluor 488 or 647 phalloidin (Molecular Probes) was used at 1:250. Wheat Germ
487 Agglutinin conjugated to alexa fluor 488 was also purchased from Molecular Probes and used at
488 1:300 to stain cell membranes.

489 Phos-tag was purchased from Wako Chemicals. Jasplakinolide (Cat #11705) and Y-
490 27632 (Cat #100005583-5) were purchased from Cayman Chemicals. DMSO (Cat #D2650),
491 Latrunculin B (Cat #L5288) and Cytochalasin D (Sigma Cat #C8273) were purchased from
492 Sigma-Aldrich. Calyculin A (Cat #BML-EI92-0100) was purchased from Enzo Life Sciences and
493 Blebbistatin (Cat #B592500) was purchased from Toronto Research Chemicals.

494 Ezrin point mutants T567E, and T567A were previously generated as described in
495 Viswanatha et al., 2012. Sequences for LOK-GFP-Flag, LOK-CTD-GFP-Flag (or LOK_310-968-
496 GFP-Flag) and LOK-K65R-GFP-Flag were also previously generated in the lab (Pelaseyed et
497 al., 2017; Viswanatha et al., 2012). To generate stable cell lines, ezrin and LOK cDNAs were
498 subcloned into pCDH lentivector (System Biosciences). Puromycin gene in pCDH was then
499 substituted for blasticidin using Gibson assembly. The lentivectors were then transfected with
500 psPAX2 and pCMV-VSVG before virus collection and transduction into Jeg-3 cells. Cells were
501 then grown under blasticidin selection at 5.0 µg/ml for 1-2 weeks prior to immunofluorescent
502 experiments. Stable expression for ezrin was validated using either an ezrin antibody for ezrin
503 constructs or GFP expression for LOK constructs.

504 **Cell culture**

505 Jeg-3, HeLa and Caco-2 cells (ATCC) were maintained in a 5% CO_2 humidified chamber
506 at 37°C. Jeg-3 cells were maintained in MEM with 10% FBS, penicillin/streptomycin and
507 GlutaMax (Thermo Fisher). Cells were cultured on Corning 100mm x 20mm cell culture
508 polystyrene dishes. HeLa and Caco-2 cells were maintained in DMEM with 10% FBS and
509 penicillin/streptomycin. Knockout cell lines were maintained with additional 2.0 µg/ml Puromycin
510 (Sigma) selection. Transient transfections were done using either Lipofectamine 3000
511 (Invitrogen) according to the manufacturer's instructions or polyetheylenimine reagent
512 (PolyPlus) as previously described (Viswanatha et al., 2012).

513 Single guide RNAs (sgRNAs) were designed using CRISPR analysis tools on Benchling
514 and cloned into puromycin-resistant pLenti-CRISPRV2 (AddGene #49535) as described in
515 Sanjana et al., 2014 and Shalem et al., 2014 (Sanjana et al., 2014; Shalem et al., 2014). The
516 following sgRNA sequences were used: 5' - GCAATGTCCGAGTTACCACCA - 3' (ezrin), 5' -
517 AGAAGCAGAACGACTTGAAA - 3' (radixin), 5' - GTAAGACTCACCCAGCATGA - 3' (LOK), 5' -
518 GCAGTACGAACACGTGAAGA - 3' (SLK). Each lentiviral construct was then transfected into
519 293TN cells with psPAX3 and pCMV-VSVG (a gift from Jan Lammerding, WICMB/Cornell,
520 Ithaca, NY) for 48-72 hours before virus collection. Target cells (Jeg3, HeLa or Caco-2) were
521 then transduced with either one or two lentiviruses in order to generate a mixed population of
522 single and double knockout cells. Cells were sorted into single cells and then expanded in
523 puromycin selection before screening by immunofluorescence and Western blotting.

524 Growth curves of Jeg3 cells were preformed by plating cells on low evaporation lid, flat
525 bottom 96 well plates (Corning Cat. #3595). Once plated, cells were seeded at 3,000 cells per
526 well. Plates were then imaged once per hour for 100hrs using a 20X objective using an Incucyte
527 Zoom v2016 (Essen BioSciences) kept in standard cell incubation chamber conditions. Raw
528 data Images were collected and analyzed using Incucyte. Graphs were assembled and
529 exported using Graphpad/Prism (version 8).

530 **Western blotting and immunoprecipitation**

531 Western Blot analysis of cell lysates were done using 6%-12% split SDS-PAGE gels
532 while 6% gel was used for phos-tag experiments. Phos-tag reagent was added at a final
533 concentration of 50uM to a standard Tris-glycine-SDS polyacrylamide gel according to the

534 manufacturer's recommendations. Gels were transferred to a PVDF membrane and blocked
535 with 5% milk in TBS + 0.5% Tween-20. Primary antibodies were incubated with the membrane
536 in 5% bovine serum albumin either for 1 hour at room temperature or overnight at 4°C. Bands
537 were detected with HRP (Thermo Fisher) or infrared fluorescent secondary antibodies
538 (Invitrogen or LI-COR Biosciences). Membranes were imaged using a scanner (Odyssey; LI-
539 COR Biosciences).

540 For detecting myosin-light-chain and phospho-myosin-light-chain, 16% or split 7.5-17.5%
541 SDS-PAGE gels were used and transferred to PVDF membranes with 0.2um pore size was
542 used (Millipour Immuoblion-P^{SQ}). The membrane was then blocked with Immobilon Block-PO
543 phosphoprotein-blocking buffer from EMD-Millipore and incubated with primary antibody
544 solution overnight before developing with chemiluminescent reagents (Radiance Q Plus, Azure
545 Biosystems) on a Bio-Rad ChemiDoc. Relative band intensities were calculated in ImageJ and
546 normalized to a loading control and exported to Graphpad/Prism for statistical analysis.
547 Caylculin A treatments for MLC Blotting were performed by incubating the drug with cells for 10
548 minutes at 37°C prior to lysis. Lysis of cells for MLC blotting was performed with warm (70°C)
549 Laemmli sample buffer, followed by immediate scraping and boiling.

550 To determine an interaction between LOK and constitutively active RhoA-L30, cells were
551 transiently co-transfected with LOK-CTD-GFP-Flag and HA-RhoA-L30 (a kind gift from the
552 Cerione lab, Cornell, Ithaca, NY). After 24 hours, cells were lysed and then solubilized in cold
553 immunoprecipitation buffer (25 mM Tris, pH 7.4, 5% glycerol, 150 mM NaCl, 50 mM NaF, 0.1
554 mM Na3VO4, 10 mM β-glycerol phosphate, 8.7 mg/ml paranitrophenylphosphate, 0.5% Triton
555 X-100, 0.1 μM calyculin A, and protease inhibitor tablet [Roche]) and immunoprecipitated for 2 h
556 using Flag M2 affinity gel (Sigma-Aldrich). Immunoprecipitates were then extensively washed in
557 immunoprecipitation wash buffer (25 mM Tris, pH 7.4, 5% glycerol, 150 mM NaCl, 50 mM NaF,
558 and 0.2% Triton X-100) and then eluted in 200 μg/ml 3×Flag peptide, denatured in Laemmli
559 buffer, resolved by SDS-PAGE, transferred to polyvinylidene difluoride, and developed with
560 HRP western detection.

561 **Active RhoA pull-down**

562 For GTP-RhoA pull down assay the Rho Activation Assay biochem kit (Cytoskeleton inc,
563 Cat# BK036) was used as described in the product manual. In summary, WT Jeg-3 or KO cell
564 lines were plated and grown for 3 days on Corning 100mm x 20mm cell culture polystyrene

565 dishes. An optimum confluency of 70-80% was used as higher confluences can result in partial
566 loss of a monolayer and disruption of apical morphology in Jeg-3 cells. Cells were lysed using
567 the kit lysis buffer and protease inhibitor cocktail then clarified at 10000 x g at 4°C for 1 min. The
568 lysate was then snap frozen in liquid nitrogen as quickly as possible to reduce RhoA-GTP
569 hydrolysis. Frozen lysates were then stored at -80°C. Protein concentrations were measured
570 using the Bradford reagent and absorption at 595nm. Upon thawing aliquots, lysate protein
571 concentration was then normalized to a uniform protein concentration using kit lysis buffer.
572 Equal concentrations of lysate were then passed on 100ug of Rhotekin-RBD beads. The beads
573 were then washed, pelleted and finally boiled with 20ul of Laemmli sample buffer. Positive and
574 negative controls using WT-Jeg 3 lysate incubated with either GTPγs or GDP for 15 minutes
575 prior to passing over the Rhotekin-RBD bead were used to confirm the detectable range of
576 western blot detection, to confirm Rho-A hydrolysis activity and Rhotekin bead binding capacity.
577 Samples were run on a 7.5-17.5% split SDS-PAGE gel and blotted for RhoA; Monoclonal
578 Mouse anti-RhoA antibody (Cytoskeleton inc. Cat#ARH05) was used at 1:500 dilution in TBST
579 overnight.

580 **Time-lapse microscopy, immunofluorescence and image analysis**

581 Cells were treated to a final concentration of 10nM calyculin A diluted into cell media
582 plus 10mM HEPES at the start of time-lapse imaging. Phase contrast images for timecourse
583 movies were taken every 4 minutes for an hour using a 20x objective on a Zeiss AXIO widefield
584 inverted microscope fitted with a 37°C temperature environmental chamber. For blebbistatin
585 experiments, blebbistatin was added to the media to a final concentration of 25uM, 30 minutes
586 prior to addition of calyculin A. For of calyculin A treatment timecourse movies and still frames,
587 imaging was started immediately before addition of calyculin A and time zero was defined as the
588 first captured frame after calyculin A addition.

589 Prior to fixation for immunofluorescence, Jeg3 cells grown on coverslips were washed
590 with PBS and pre-stained with WGA at 1:300 for 30 minutes. For actin turnover experiments in
591 Figure 5A, Jeg3 cells were treated with either DMSO, 500nM Jasplakinolide or 100ng/mL
592 Latrunculin B for 30 min, prior to fixation. Otherwise, for all other immunofluorescent
593 experiments, cells grown on glass coverslips were fixed in 3.7% formalin/PBS for 15 min at
594 room temperature. Cells were then washed with PBS and blocked with immunofluorescence
595 buffer (PBS + 0.5% BSA + 0.5% goat serum + 0.1% Triton X-100) for 10 min. Primary and
596 secondary antibodies were then applied in immunofluorescence buffer containing 2% FBS.

597 Alexa Fluor–conjugated phalloidin, was added to the secondary. The cells were mounted in
598 SlowFade Diamond Antifade (Thermo Fisher) and imaged using a spinning-disk (Yokogawa
599 CSU-X1; Intelligent Imaging Innovations) Leica DMi600B microscope with spherical aberration
600 correction device and a 100/1.46 numerical aperture Leica objective. Images were acquired with
601 a metal-oxide semiconductor device camera (sCMOS) and image slices were assembled using
602 SlideBook 6 software (Intelligent Imaging Innovations). Maximum or summed intensity
603 projections were assembled in SlideBook 6 and exported to Illustrator software (Adobe). For
604 clarity, side projections were vertically expanded using Illustrator. Deconvolution images were
605 captured using an inverted Leica DMi8 wide-field microscope equipped a Leica 506249
606 100X/1.49 oil objective, Leica DFC 9000 GTC camera, with Leica application suit X thunder
607 deconvolution software.

608 The presence or absence of microvilli was scored as described previously (Garbett et
609 al., 2010; Hanono et al., 2006; LaLonde et al., 2010; Pelaseyed et al., 2017; Sauvanet et al.,
610 2015). More than 50 cells per replicate were stained using the WGA, ezrin and phalloidin and
611 binned into two categories: microvilli and no microvilli. Microvilli above cell–cell junctions were
612 ignored in the scoring.

613 For calculating tortuosity among tight junctions and relative apical and lateral actin
614 intensities, cells were stained with a ZO-1 antibody and phalloidin and imaged on a spinning-
615 disk microscope as described earlier. To analyze tortuosity, the ZO-1 channel was skeletonized
616 into 1 pixel line widths using ImageJ. Between two consecutive intersection points, a straight-
617 line length was measured and the average of two manually traced line lengths (to account for
618 human variability) along the skeletonized line were also measured. From there, the ratio
619 between the actual line length to the expected line length (straight length) was calculated and
620 exported into Graphpad/Prism for statistical analysis. For comparing actin intensities between
621 apical and lateral regions, Max-Z projections were divided between ZO-1 positive (apical) and
622 ZO-1 negative (lateral) staining. From there, outlines of each cell were traced and measured for
623 their relative mean intensity value in the apical stacks versus the lateral stacks. The ratio
624 between the apical and lateral values were then calculated, plotted and analyzed for statistical
625 significance (Welch's t-test) in GraphPad/Prism.

626 **Atomic Force Microscopy (AFM)**

627 Atomic force microscopy experiments were performed using a MFP-3D-BIOTM Atomic
628 Force Microscope by Asylum Research mounted on an Olympus IX71 inverted microscope that
629 resides on a Herzan AVI 350-S Active Vibration Isolation Table totally enclosed in an air tight
630 BCH-45 Large Acoustic Isolation Hood. Software modules are written in Igor Pro by
631 Wavemetrics. Cells were plated onto WillCo-Dish Glass bottom dish (size 50x7mm. glass
632 30mm. Class #1.5, 0.17mm (Product number GWST-5030; Willco Wells)). Pyramidal shaped
633 Probe TIP (PNP-TR-20) from Asylum Research (804.NW.PNP-TR) were used and calibrated
634 using an in-air calculation of the spring constant. Individual cells within monolayers were
635 selected using phase contrast live imaging with the probe tip location simultaneously illuminated
636 onto the field of view. Probe tips were lowered onto a cell at a velocity of 1000nm/s to a trigger
637 point of 1 nN. Individual cells were force mapped by indenting 100 times over a square 20μm x
638 20μm area. Simultaneous force indentation and membrane retraction measurements were
639 made by first incubating probe tips with 3.0mg/ml of concanavalin A in PBS buffer for 1.5 hours
640 at room temperature. Deflection and z-probe position data was exported into matlab then
641 analyzed using the open access software from Huth and colleagues (Huth et al., 2019) modified
642 for a pyramidal shape probe tip. Force indentation traces were filtered for single force peaks
643 then chi-value goodness fit to the Hertz model. Youngs modulus statistical analysis and
644 graphing of AFM data was performed in Graphpad/Prism.
645

646 **Acknowledgements**

647 We thank the University of Vermont College of Medicine Microscopy Imaging Center,
648 specifically D. Taatjes and N. Bouffard for their help using the Asylum Research MFP-3 D BIO
649 atomic force microscope. The microscope was purchased with support from NIH award number
650 S10RR025498 from the National Center for Research Resources (to DT). We thank Alan Howe,
651 Robert Bauer and Albert van der Vliet (University of Vermont) for their help with AFM data
652 collection and suggestions on Myosin Light Chain detection and Steven Huth (Christian-
653 Albrechts University of Keil) for his help implementing AFM Hertz fit analysis to our data. We
654 thank Jan Lammerding (Cornell University) for his generosity with reagents and use of
655 equipment and Adam Martin (MIT) for his helpful discussions and reviewing the manuscript. We
656 appreciate the effort by Shannon Marshall and Marcus Smolka (Cornell University) with
657 attempts to identify additional LOK phosphorylation targets. A.T.L. was supported by a Fleming
658 Research Fellowship. This work was supported by NIH Grants RO1 GM036552 and R35
659 GM131751 to A.B.

Figures

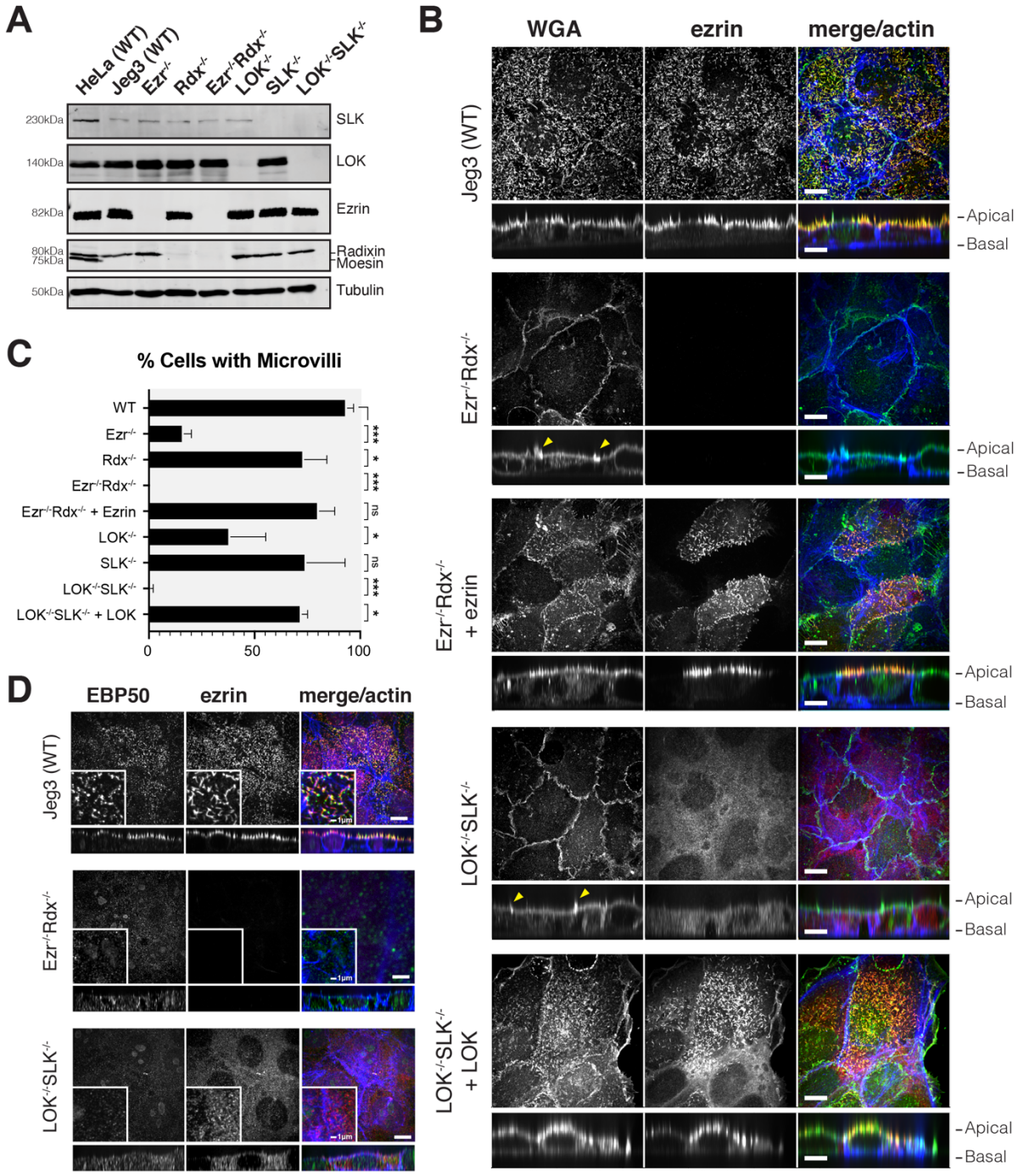
A
HeLa (WT)
Jeg3 (WT)
Ezr-/-
Rdx-/-
Ezr-/-Rdx-/-
LOK-/-
SLK-/-
LOK-/-SLK-/-
230kDa
SLK
140kDa
LOK
82kDa
Ezrin
80kDa
75kDa
Radixin
Moesin
50kDa
Tubulin
B
WGA
ezrin
merge/actin
Jeg3 (WT)
Ezr-/-Rdx-/-
Ezr-/-Rdx-/- + ezrin
LOK-/-SLK-/-
LOK-/-SLK-/- + LOK
Apical
Basal
C
% Cells with Microvilli
WT
Ezr-/-
Rdx-/-
Ezr-/-Rdx-/-
Ezr-/-Rdx-/- + Ezrin
LOK-/-
SLK-/-
LOK-/-SLK-/-
LOK-/-SLK-/- + LOK
***
*
***
ns
*
ns
***
*
0
50
100
D
EBP50
ezrin
merge/actin
Jeg3 (WT)
Ezr-/-Rdx-/-
LOK-/-SLK-/-
1µm

Figure 1: Jeg3 cells lacking ERM proteins or LOK/SLK are viable and lack microvilli. (A) Protein expression using indicated antibodies in western blots of ERM proteins and LOK and SLK in Jeg3 CRISPR cell lysates. HeLa cell lysate was used as a control for expression of moesin, which is not present in Jeg3. Tubulin expression was used as a loading control. (B) Jeg3 cell lines lacking ERM expression or LOK and SLK expression were stained with Wheat-Germ-Agglutinin (WGA), ezrin and actin. Yellow arrows indicate strong membrane ruffles. (C) Percentage of cells expressing microvilli. Bars represents mean±SEM, N=3. Non-significant (ns) p-values are as follows: Ezr $^{-/-}$ Rdx $^{-/-}$ + ezrin = 0.0770 ; LOK $^{-/-}$ SLK $^{-/-}$ + LOK = 0.2079. (D) Staining of cells with EBP50, ezrin and actin in the indicated cells. Scale bars, 10μm unless otherwise noted. Vertical sections were expanded three-fold for clarity. P-values were calculated with Welch's t-test (* $p \leq 0.05$, ** $p \leq 0.01$, *** $p \leq 0.001$).

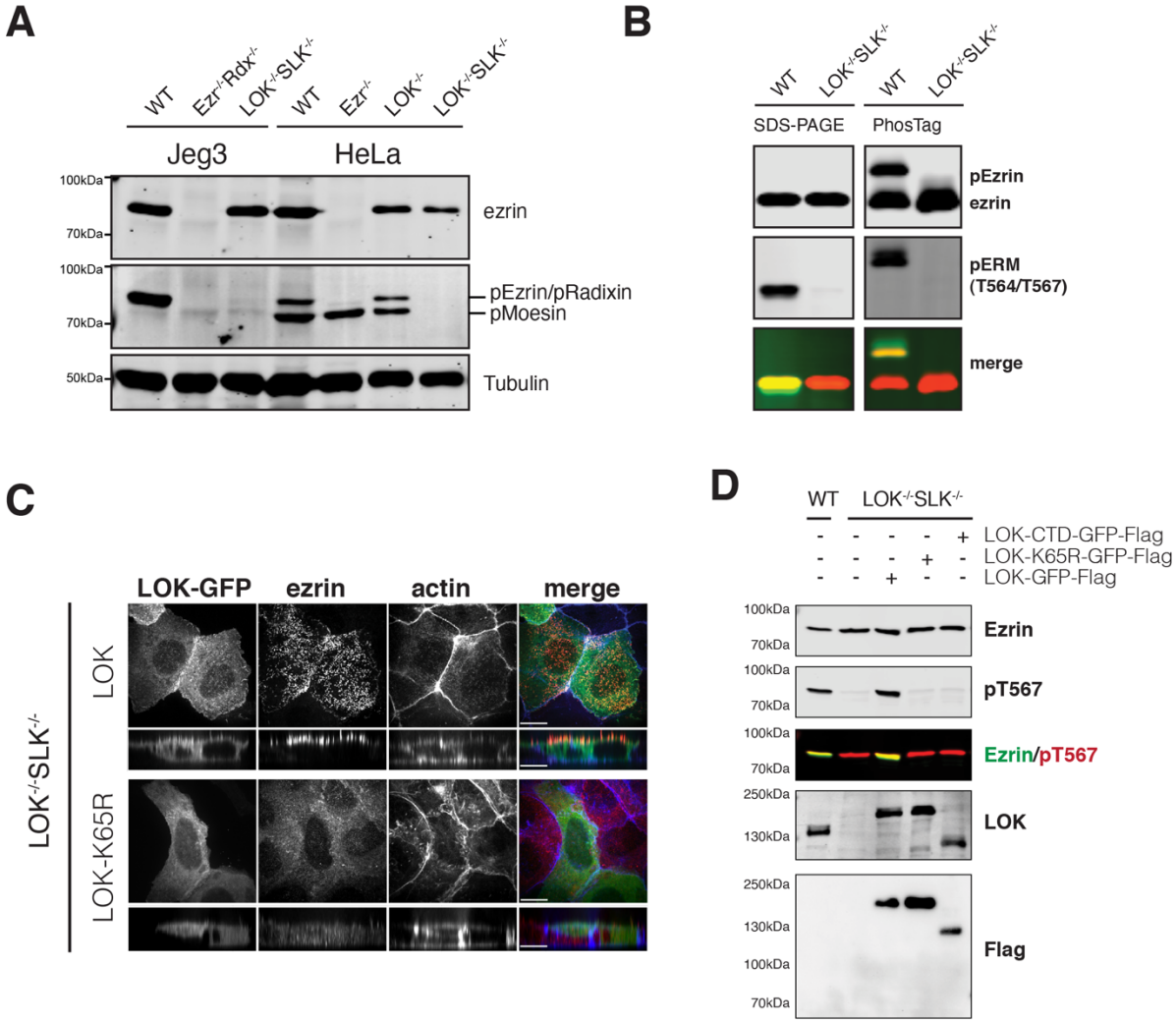
A
WT
Ezr-/-Rdx-/-
LOK-/-SLK-/-
WT
Ezr-/-
LOK-/-
LOK-/-SLK-/-
Jeg3
HeLa
100kDa
70kDa
ezrin
100kDa
70kDa
pEzrin/pRadixin
pMoesin
50kDa
Tubulin
B
WT
LOK-/-SLK-/-
WT
LOK-/-SLK-/-
SDS-PAGE
PhosTag
pEzrin
ezrin
pERM
(T564/T567)
merge
C
LOK-GFP
ezrin
actin
merge
LOK-/-SLK-/-
LOK
LOK-K65R
D
WT
LOK-/-SLK-/-
- - - - + LOK-CTD-GFP-Flag
- - - + - LOK-K65R-GFP-Flag
- - + - - LOK-GFP-Flag
100kDa
70kDa
Ezrin
100kDa
70kDa
pT567
100kDa
70kDa
Ezrin/pT567
250kDa
130kDa
LOK
250kDa
130kDa
100kDa
70kDa
Flag

Figure 2: LOK/SLK are the major ERM kinases. (A) Ezrin and phospho-ERM levels in Jeg3 or HeLa knockout cells. Tubulin is used as a loading control. (B) Extracts of wildtype or $LOK^{-/-}SLK^{-/-}$ cells were resolved by either 6% SDS-PAGE gel or 6% Mn-Phos-Tag SDS-PAGE gel and blotted for ezrin and phosphoERM. Approximately half of endogenous ezrin is phosphorylated in wildtype cells as seen by the shift in band size. No phospho-shift is detected in $LOK^{-/-}SLK^{-/-}$ cells. (C) $LOK^{-/-}SLK^{-/-}$ cells transfected with either LOK-GFP-flag or K65R-LOK-GFP-flag and then co-stained with ezrin and actin. K65R-LOK is unable to rescue apical ezrin localization. (D) Extracts of cells transfected with wildtype LOK or LOK mutants were collected and blotted for endogenous ezrin or phosphoERM. Lysates were also blotted for flag or LOK to check expression of the constructs relative to wildtype LOK. Scale bars 10μm.

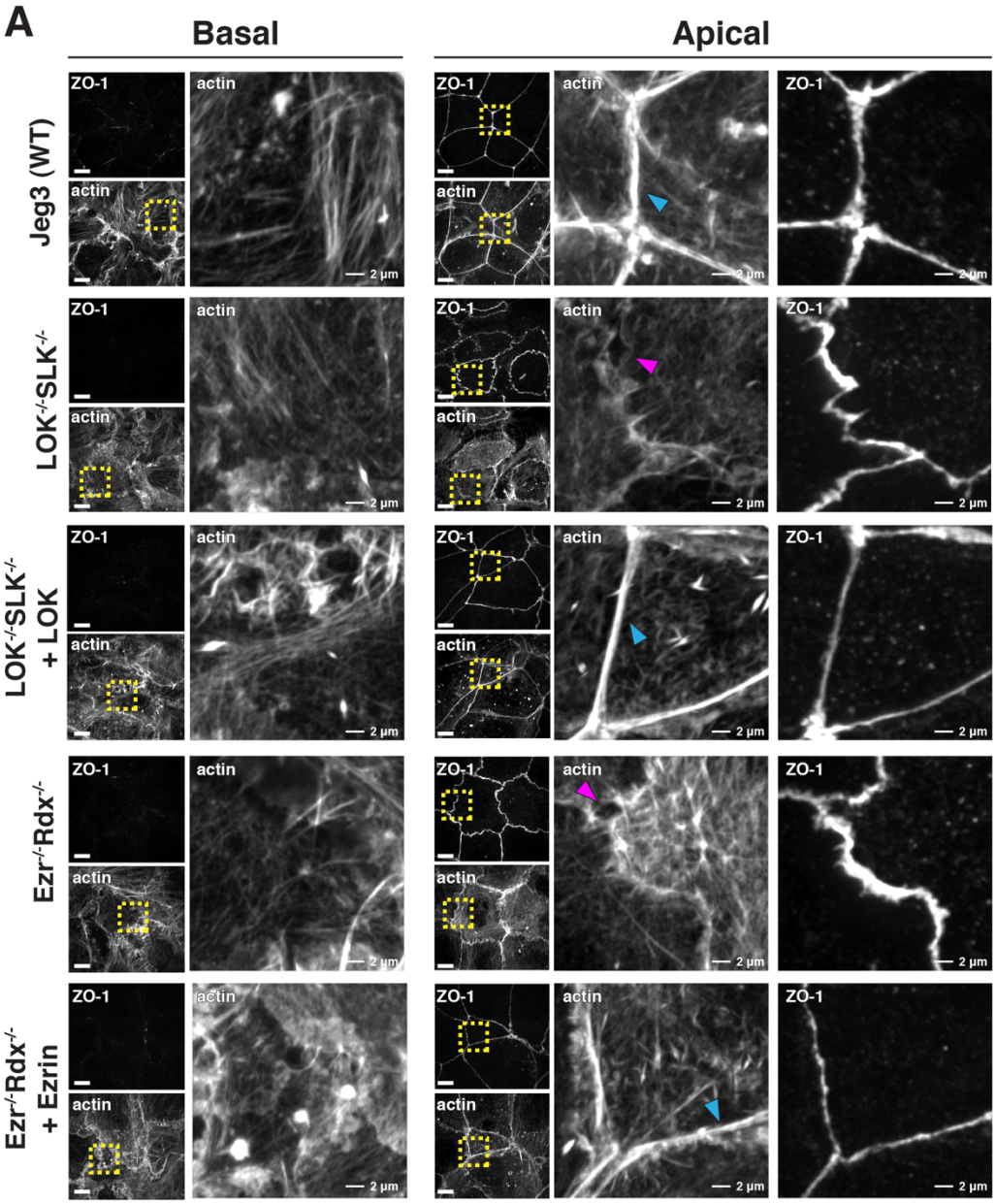
A
Basal
Apical
Jeg3 (WT)
LOK-/-SLK-/-
LOK-/-SLK-/- + LOK
Ezr-/-Rdx-/-
Ezr-/-Rdx-/- + Ezrin
ZO-1
actin
2 µm

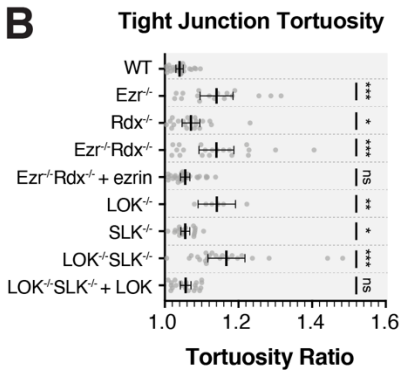
B
Tight Junction Tortuosity
WT
Ezr-/-
Rdx-/-
Ezr-/-Rdx-/-
Ezr-/-Rdx-/- + ezrin
LOK-/-
SLK-/-
LOK-/-SLK-/-
LOK-/-SLK-/- + LOK
***
*
***
ns
**
*
***
ns
1.0
1.2
1.4
1.6
Tortuosity Ratio

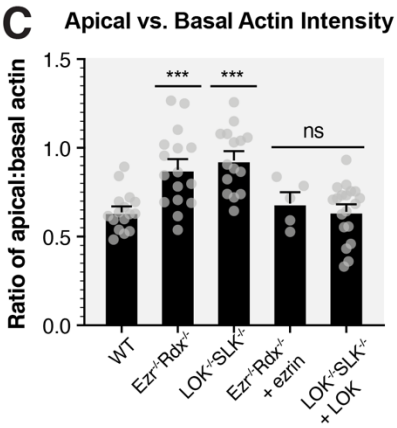
C
Apical vs. Basal Actin Intensity
Ratio of apical:basal actin
1.5
1.0
0.5
0.0
***
***
ns
WT
Ezr-/-Rdx-/-
LOK-/-SLK-/-
Ezr-/-Rdx-/- + ezrin
LOK-/-SLK-/- + LOK

Figure 3: Absence of activated ERM proteins induces the formation of apical actin bundles, alters cell-cell junctions, and compromises the apical rigidity of epithelial cells. (A) Comparison of ZO-1 and actin between basolateral and apical confocal slices. Apical Z-slices were determined by the presence of ZO-1. Blue arrows indicate actin present at cell junctions. Magenta arrows point to actin breaks between neighboring cells. Scale 10μm unless otherwise noted. (B) Quantification of tight junction tortuosity using ZO-1 staining. Each point represents the tortuosity from one tight junction intersection to the next intersection. Center lines respresent mean±SEM. Non-significant (ns) p-values are as follows: Ezr $^{-/-}$ Rdx $^{-/-}$ + ezrin = 0.0578 ; LOK $^{-/-}$ SLK $^{-/-}$ + LOK = 0.0573. (C) The ratios of relative mean actin intensity values per cell between apical and basolateral cross-sections. Bars represent mean±SEM. Non-significant p-values are as follows: Ezr $^{-/-}$ Rdx $^{-/-}$ + ezrin = 0.4188 ; LOK $^{-/-}$ SLK $^{-/-}$ + LOK = 0.9555. P-values were calculated with Welch's t-test (* $p \leq 0.05$, ** $p \leq 0.01$, *** $p \leq 0.001$).

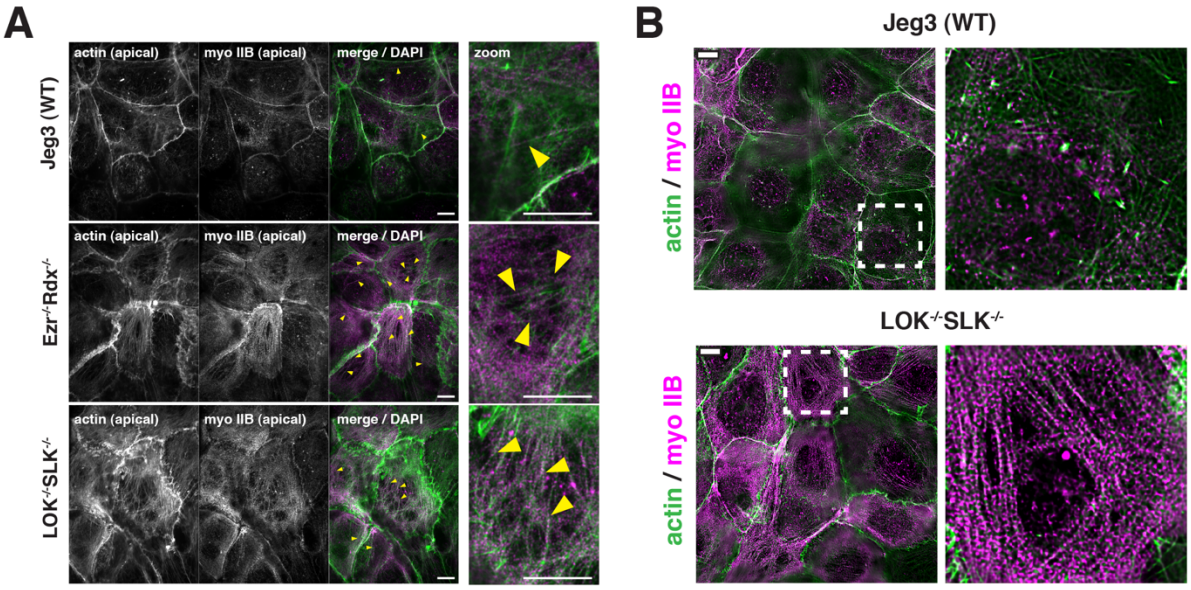
A
actin (apical)
myo IIB (apical)
merge / DAPI
zoom
Jeg3 (WT)
Ezr-/-Rdx-/-
LOK-/-SLK-/-
B
Jeg3 (WT)
actin / myo IIB
LOK-/-SLK-/-

Figure 4: A dense actomyosin network forms at the apical surface of ERM and LOK/SLK knockout cells (A) Maximum projection of immunofluorescence images of the apical confocal Z-slices (2.8μm or 10 confocal slices) indicating actin and non-muscle myosin IIB localization. Areas with contractile fibers are indicated by yellow arrows. (B) Similar apical max projection from deconvolution imaging of the same samples as in (A) showing numerous non-muscle myosin puncta along the apical actin bundles in LOK/SLK knockout cells. Scale bars 10μm.

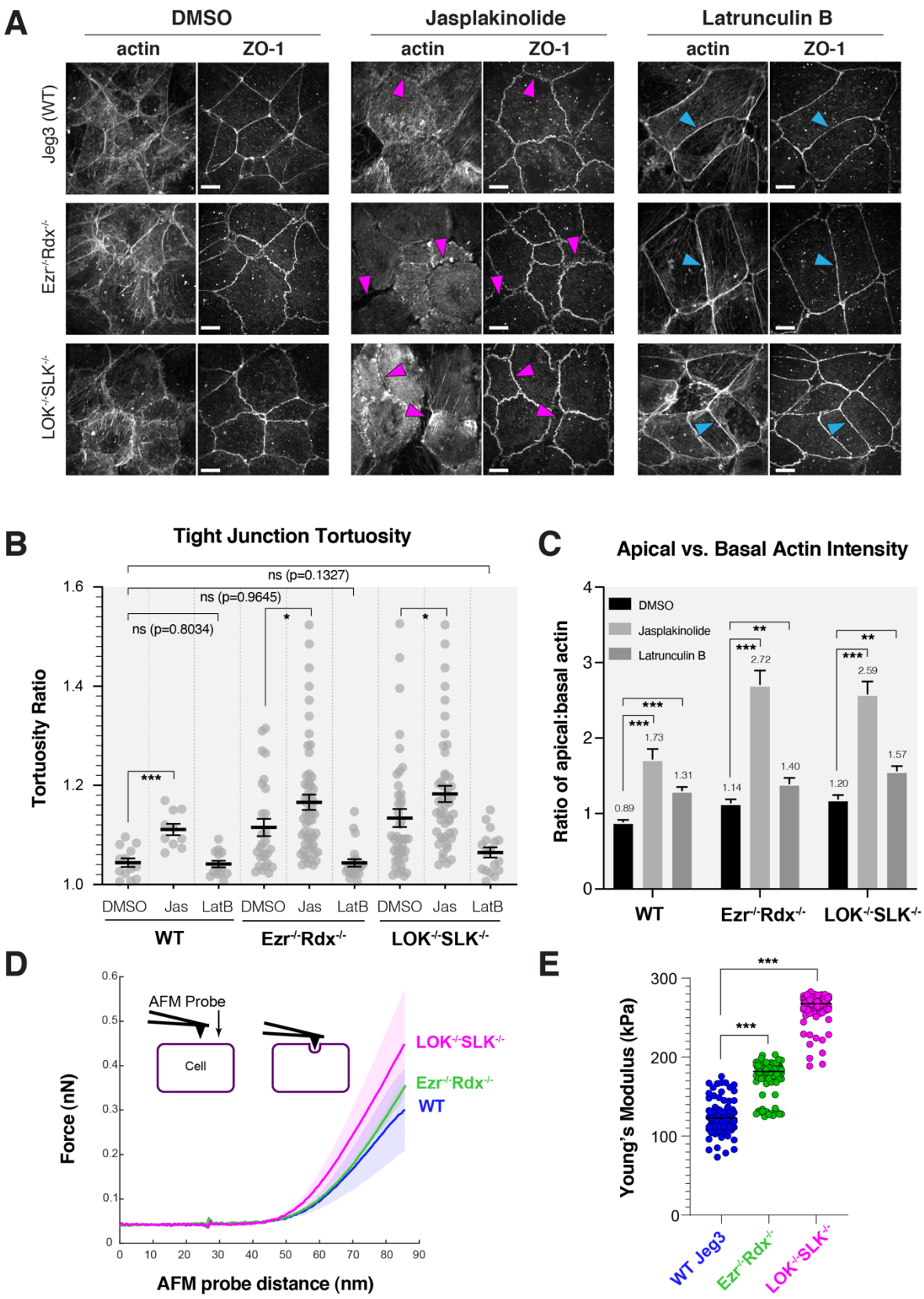
A
DMSO
Jasplakinolide
Latrunculin B
actin
ZO-1
Jeg3 (WT)
Ezr-/-Rdx-/-
LOK-/-SLK-/-
B
Tight Junction Tortuosity
Tortuosity Ratio
ns (p=0.1327)
ns (p=0.9645)
ns (p=0.8034)
DMSO
Jas
LatB
WT
Ezr-/-Rdx-/-
LOK-/-SLK-/-
C
Apical vs. Basal Actin Intensity
Ratio of apical:basal actin
DMSO
Jasplakinolide
Latrunculin B
0.89
1.73
1.31
1.14
2.72
1.40
1.20
2.59
1.57
D
AFM Probe
Cell
Force (nN)
AFM probe distance (nm)
LOK-/-SLK-/-
Ezr-/-Rdx-/-
WT
E
Young's Modulus (kPa)
WT Jeg3
Ezr-/-Rdx-/-
LOK-/-SLK-/-

Figure 5: Increased actin polymerization in ERM or LOK/SLK knockout cells leads to junctional defects and mechanical stiffening of the cell. (A) Jeg3 cells treated with DMSO, 500nM Jaspakinolide or 100ng/mL Latrunculin B for 30 min before immunostaining with ZO-1 and actin. Magenta arrows point to actin gaps at junctions while blue arrows represent actin present at cell junctions. Scale bars, 10 µm. (B) Quantification of tortuosity between tight junction markers as described in Figure 3. Jasplakinolide treatment increases tortuosity values, while Latrunculin B rescues tortuosity to wildtype levels. N ≥ 10 cells per condition. Lines represent mean±SEM. P-values were calculated with Welch's t-test (* $p \leq 0.05$, ** $p \leq 0.01$, *** $p \leq 0.001$). (C) Comparison of actin levels between apical and basolateral regions after treatment with drugs as visualized in panel A. N ≥ 21 cells per condition. Bars show mean±SEM. (D) Averaged force indentation curves for WT Jeg3 (blue), ezrin$^{-/-}$radixin$^{-/-}$ (green) and LOK$^{-/-}$ SLK$^{-/-}$ (magenta); semi-transparent area around each line represents the SEM of the data. A steeper curve indicates a stiffer cell. (E) Young's modulus stiffness parameters; black line indicates each condition's mean value (WT N=356, ezrin$^{-/-}$radixin$^{-/-}$ N=304, LOK$^{-/-}$ SLK$^{-/-}$ N=431). Both KO conditions were significantly stiffer than WT cells (*** $p=<0.0001$, K/S Test).

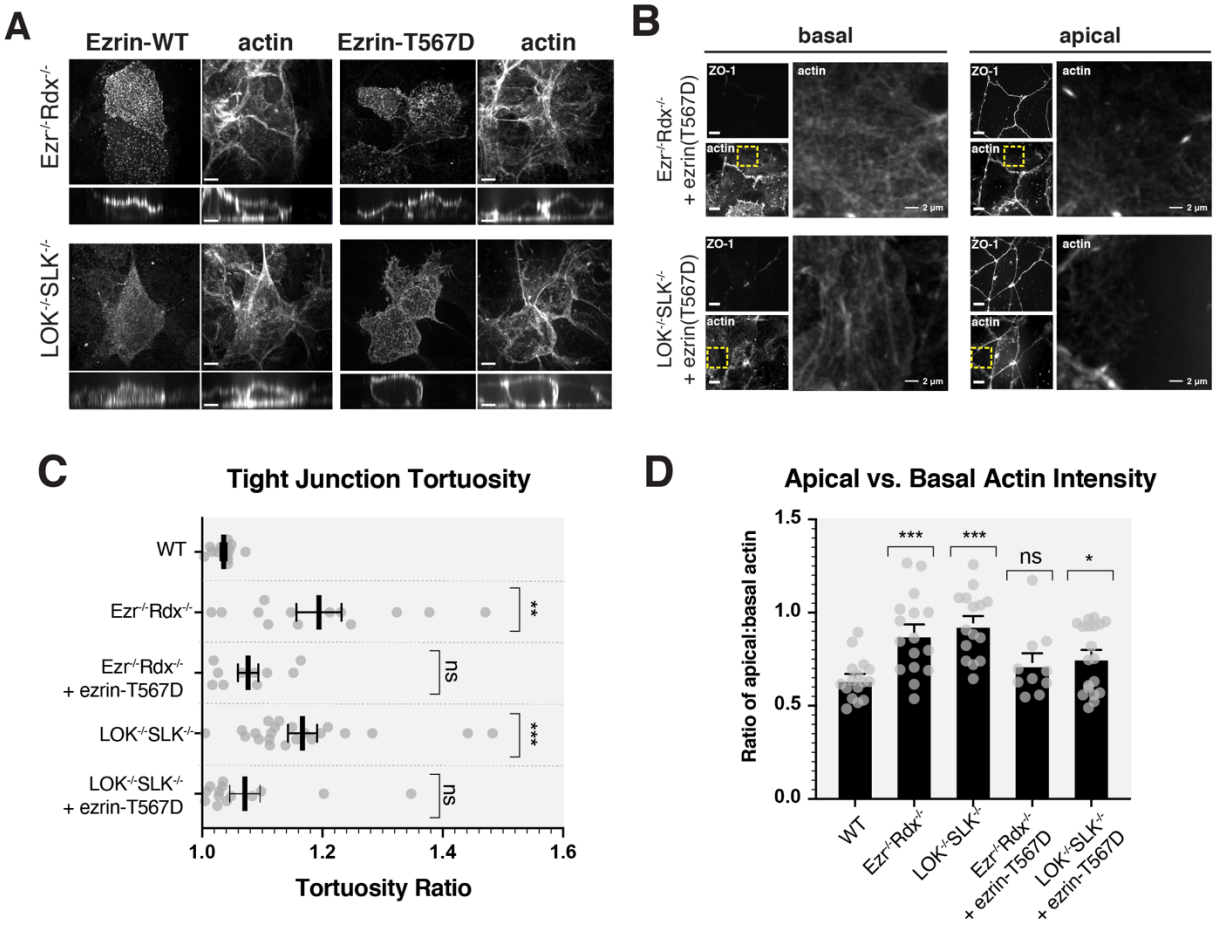
A
Ezrin-WT
actin
Ezrin-T567D
actin
Ezr-/-Rdx-/-
LOK-/-SLK-/-
B
basal
apical
ZO-1
actin
Ezr-/-Rdx-/- + ezrin(T567D)
LOK-/-SLK-/- + ezrin(T567D)
2 µm
C
Tight Junction Tortuosity
WT
Ezr-/-Rdx-/-
Ezr-/-Rdx-/- + ezrin-T567D
LOK-/-SLK-/-
LOK-/-SLK-/- + ezrin-T567D
**
ns
***
ns
1.0
1.2
1.4
1.6
Tortuosity Ratio
D
Apical vs. Basal Actin Intensity
Ratio of apical:basal actin
1.5
1.0
0.5
0.0
***
***
ns
*
WT
Ezr-/-Rdx-/-
LOK-/-SLK-/-
Ezr-/-Rdx-/- + ezrin-T567D
LOK-/-SLK-/- + ezrin-T567D

Figure 6: Constitutively active ezrin rescues apical actin distribution in knockout cells. (A) Jeg3 knockout cells expressing wildtype ezrin or T567 phosphomimetic were stained for ezrin and actin. Maximum intensity projections and vertical cross-sections are shown. (B) Comparison of ZO-1 and actin between basolateral and apical confocal slices between Jeg-3 knockout cells expressing phosphomimetic ezrin-T567D. Apical Z-slices were determined by the presence of ZO-1. Yellow boxes indicate the region of the image that was expanded on the right. (C) Quantification of tight junction tortuosity using ZO-1 staining. N ≥ 10 cells per condition. Center lines show mean±SEM. Non-significant (ns) p-values are as follows: Ezr $^{-/-}$ Rdx $^{-/-}$ + ezrin-T567D = 0.0623; LOK $^{-/-}$ SLK $^{-/-}$ + ezrin-T567D = 0.2445 (D) The ratios of relative mean actin intensity values per cell between apical and basolateral cross-sections. N ≥ 21 cells per condition. Non-significant p-value for Ezr $^{-/-}$ Rdx $^{-/-}$ + ezrin-T567D = 0.4188. Bars show mean±SEM. P-values were calculated against wildtype with Welch's t-test (* p≤0.05, ** p≤0.01, *** p≤0.001). Scale bars, 10μm; unless otherwise noted.

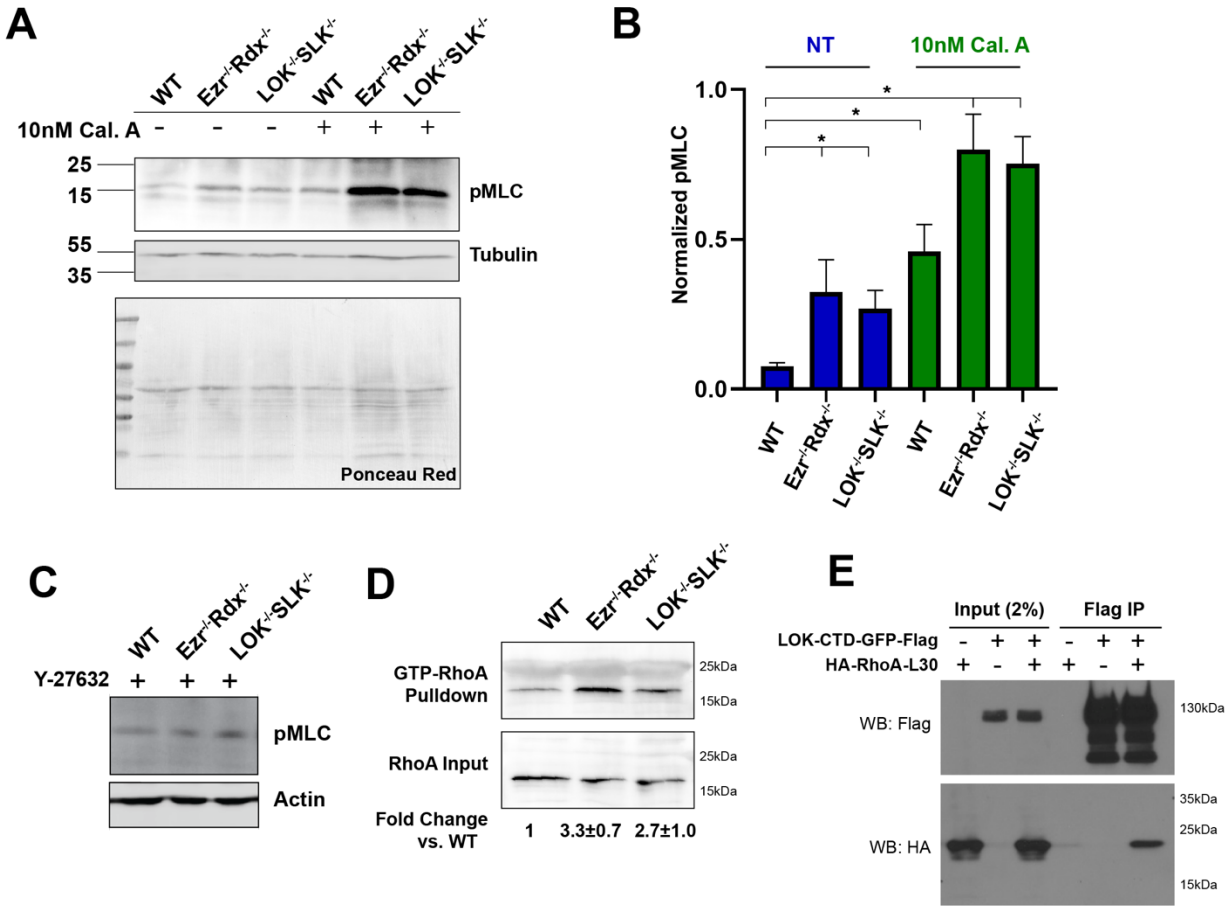
A
WT
Ezr-/-Rdx-/-
LOK-/-SLK-/-
WT
Ezr-/-Rdx-/-
LOK-/-SLK-/-
10nM Cal. A
- - - + + +
25
15
pMLC
55
35
Tubulin
Ponceau Red
B
NT
10nM Cal. A
Normalized pMLC
1.0
0.5
0.0
*
*
*
WT
Ezr-/-Rdx-/-
LOK-/-SLK-/-
WT
Ezr-/-Rdx-/-
LOK-/-SLK-/-
C
WT
Ezr-/-Rdx-/-
LOK-/-SLK-/-
Y-27632 + + +
pMLC
Actin
D
WT
Ezr-/-Rdx-/-
LOK-/-SLK-/-
GTP-RhoA Pulldown
25kDa
15kDa
RhoA Input
25kDa
15kDa
Fold Change vs. WT
1 3.3±0.7 2.7±1.0
E
Input (2%)
Flag IP
LOK-CTD-GFP-Flag - + + - + +
HA-RhoA-L30 + - + + - +
WB: Flag
130kDa
WB: HA
35kDa
25kDa
15kDa
F
RhoA-GTP
LOK/SLK
ROCK
LIMK
Cofilin
F-actin
pERM
MLC
PP1
Mypt1

Figure 7: Phosphorylated ERMs negatively regulate myosin activation through RhoA. (A) Phospho-myosin light chain (pMLC) (T18/S19) western blot with tubulin and total protein staining to indicate equal loading. (B) Quantification of pMLC staining normalized to loading control (bars show mean±SEM; control:N = 4; 10 min of 10nM CalA: N = 3). (C) Western blot of pMLC with actin loading control in Jeg3 cells first treated with ROCK inhibitor Y-27632 showing reversal of the pMLC hyperphosphorylation phenotype in KO cells. (D) Representative Western blot of active RhoA-GTP pull down results. Upper row: Rho-A blot of the Rhotekin beads following pulldown, Lower row: blot of Rho-A of 4% of input lysate. Normalized fold change of the RhoA pull down band intensity compared to WT (mean±SEM; N = 5). (E) LOK-CTD-GFP-Flag pulldown of cells expressing constitutively active RhoA (RhoA-L30) indicating that C-term LOK binds active RhoA. (F) Model of Rho A signaling negatively regulated by phospho-ERMs (dotted blue line).

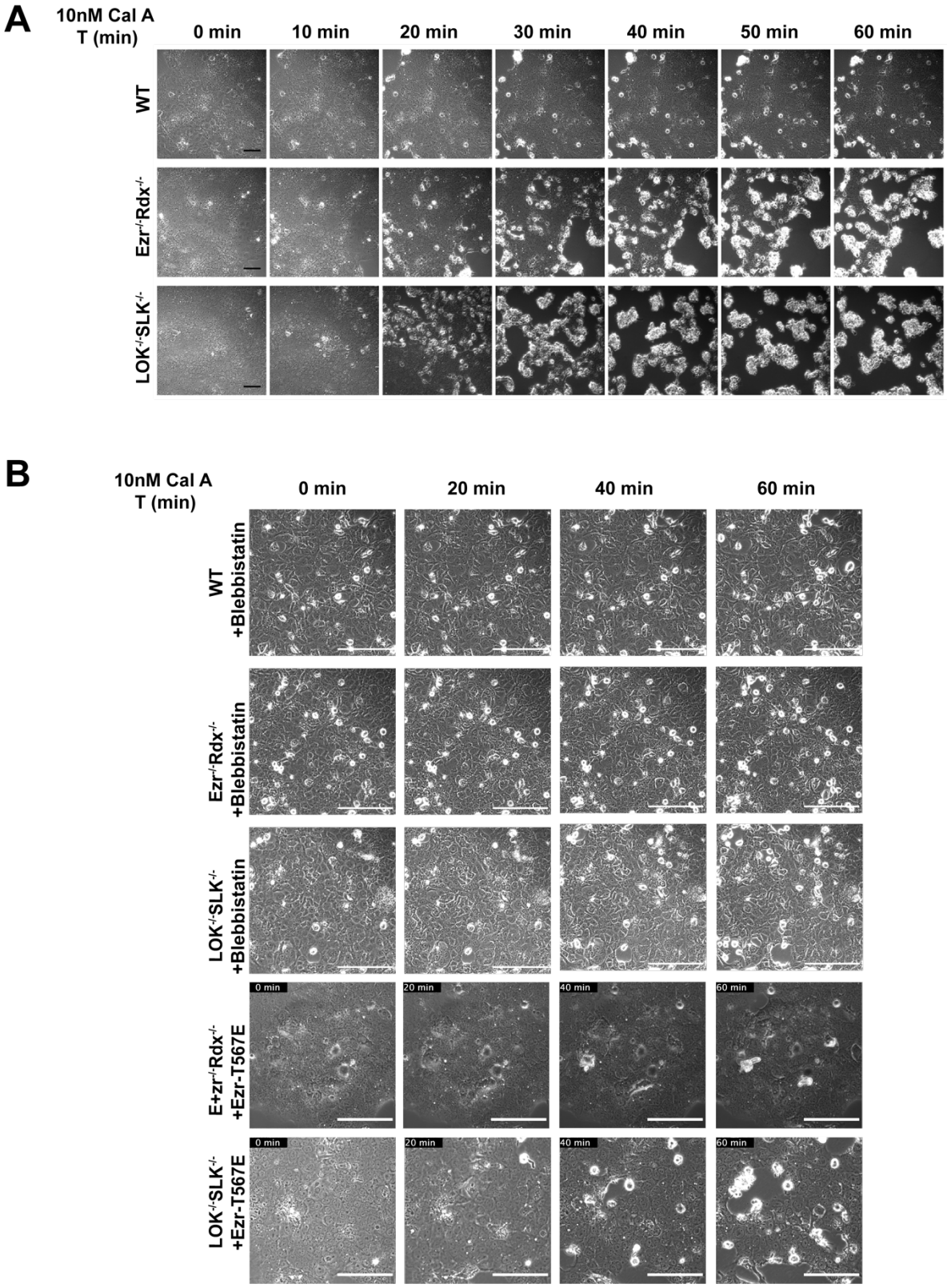
A
10nM Cal A
T (min)
0 min
10 min
20 min
30 min
40 min
50 min
60 min
WT
Ezr-/-Rdx-/-
LOK-/-SLK-/-
B
10nM Cal A
T (min)
0 min
20 min
40 min
60 min
WT +Blebbistatin
Ezr-/-Rdx-/- +Blebbistatin
LOK-/-SLK-/- +Blebbistatin
E+zr-/-Rdx-/- +Ezr-T567E
LOK-/-SLK-/- +Ezr-T567E

Figure 8: Phosphorylated ERMs negatively regulate myosin contractility. (A) Representative phase contrast still images from movies (S1) showing the effect of 10nM calyculin A on WT or KO Cells. (B) Same as (A) except for 30 min treatment with 25uM blebbistatin (Movie S2), or transfection to express phosphomimetic ezrin-T567E (Movie S3), prior to calyculin A treatment. Scales 100μm.

SUPPLEMENTAL MATERIALS

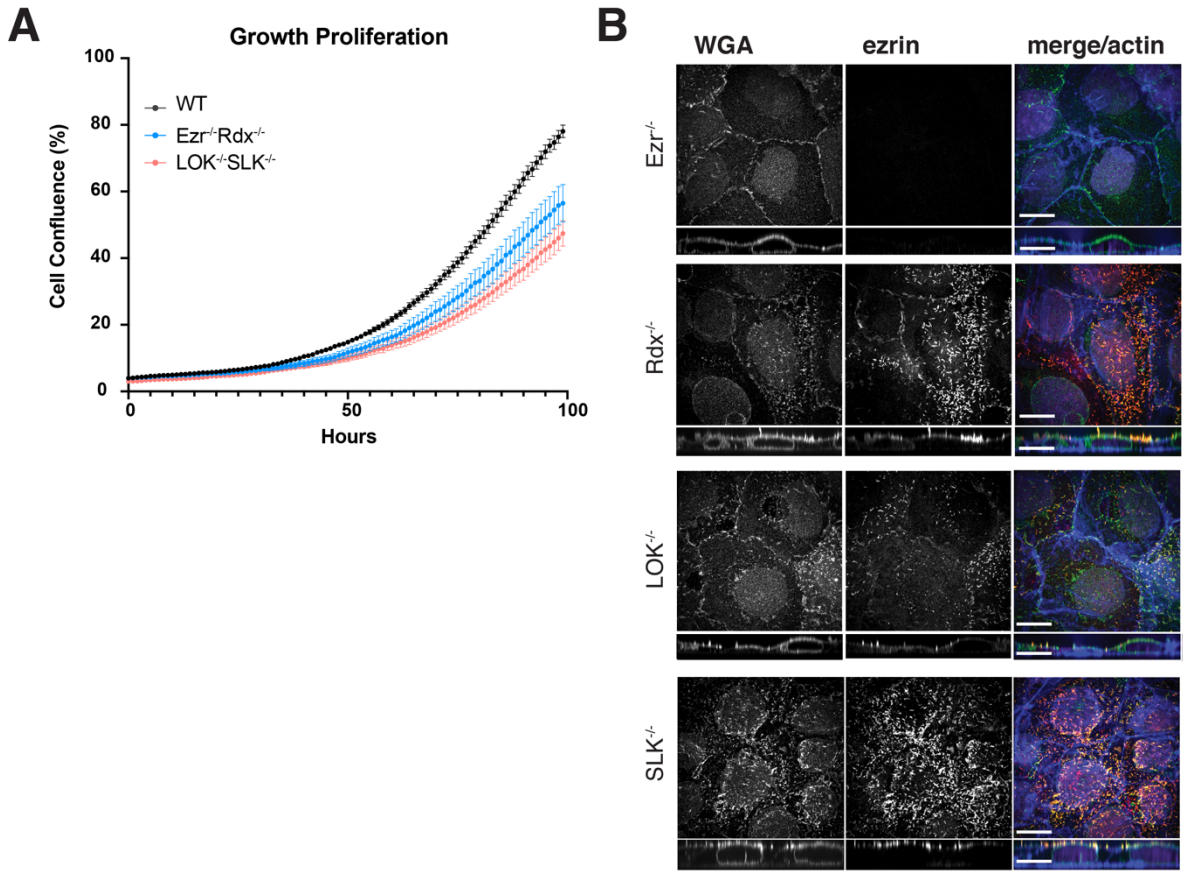

Figure S1: Single KO phenotypes in Jeg3 cells. (A) Growth curve WT (grey) vs. Ezr$^{-/-}$Rad$^{-/-}$ (Blue) and LOK$^{-/-}$SLK$^{-/-}$ cells (orange). N=15 wells of cells shown WT ; N=15 Ezr$^{-/-}$Rad$^{-/-}$; N=15 LOK$^{-/-}$SLK$^{-/-}$. 3,000 cells were seeded per well on 96-well plates and imaged every hour using Incucyte Live-cell analysis system. Each point represents cell confluence, measured by Incucyte over time per hour, from 0 to 100 hours. Error bars = SEM (B) Representative immunofluorescent staining of microvilli in single KO cells used for microvilli quantification and assessment of partial defects.

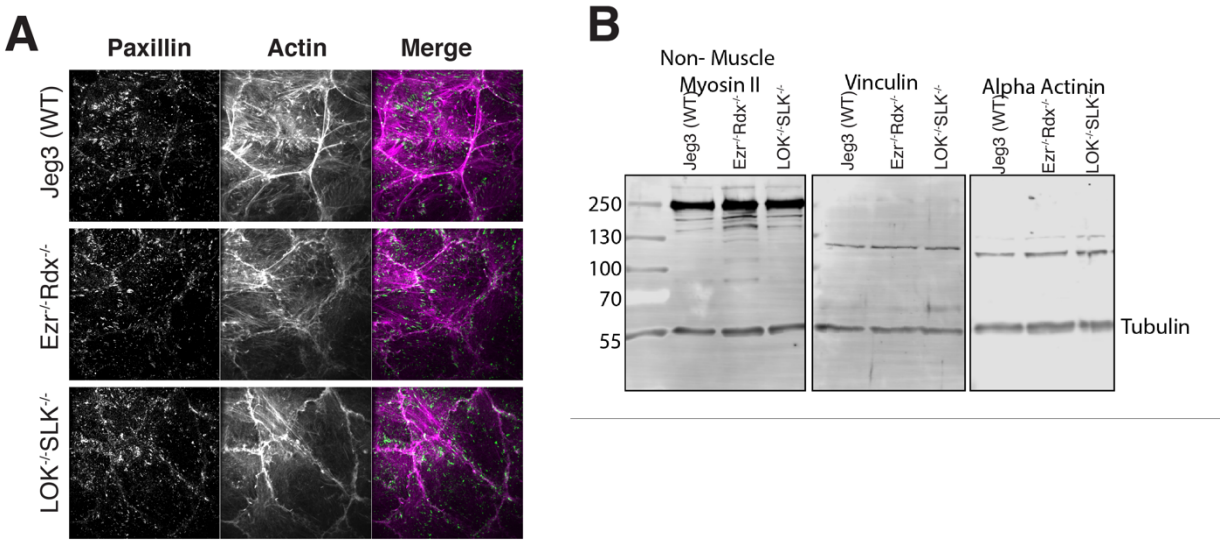

Figure S2: Focal contacts in WT Jeg3 vs LOK$^{-/-}$SLK$^{-/-}$, Ezr$^{-/-}$Rad$^{-/-}$ cells. (A) Immunofluorescent staining of Paxillin focal adhesion marker and actin shows similar organization. (B) Western blotting of Non-Muscle Myosin II, Vinculin and alpha-actinin and tubulin in Jeg3 WT and double knockout cells.

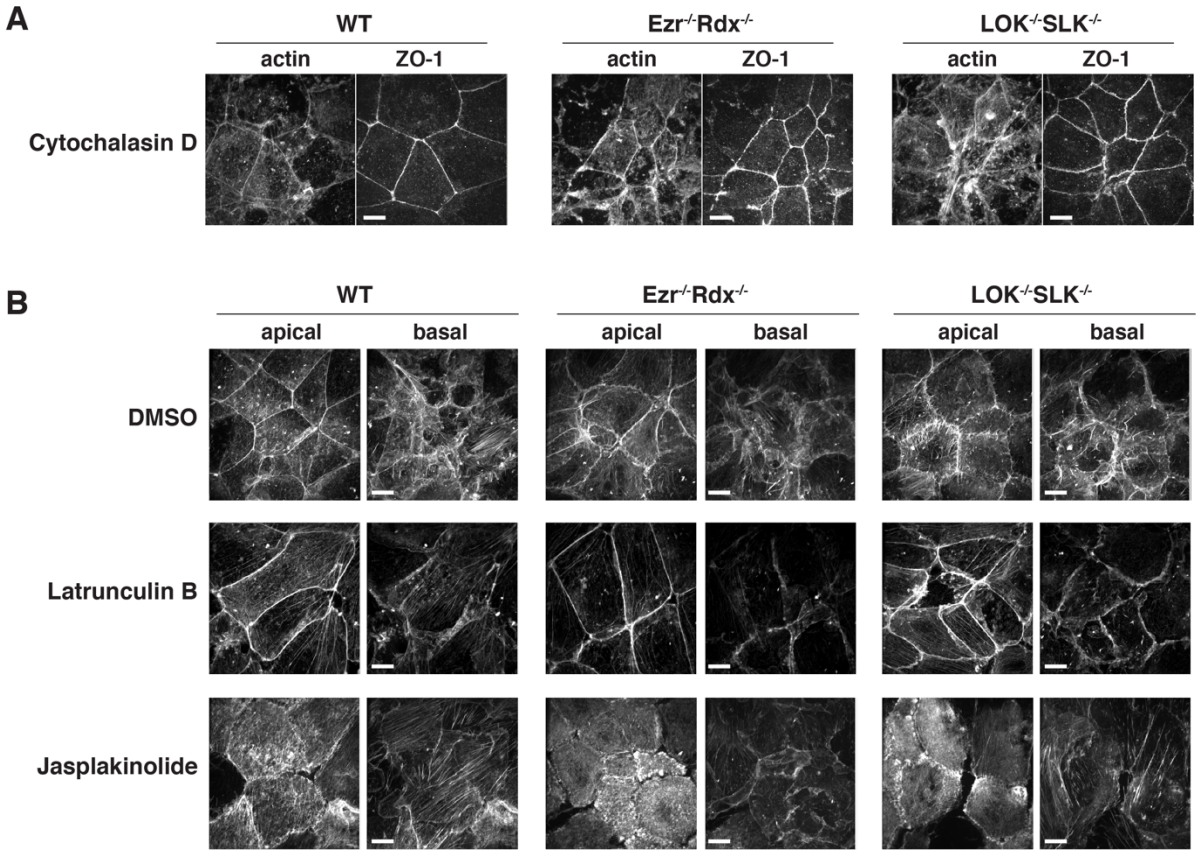

Figure S5: Effects of actin polymerizing drugs on Jeg-3 epithelial cells. (A) Jeg3 cells treated with 1µg/mL of Cytochalasin D for 30 min prior to fixation and staining with ZO-1 and actin. (B) Actin staining of apical and basolateral slices from maximum projection images in Figure 5A. Notably, Latrunculin B treatment favors disassembly of basolateral actin over apical actin, while maintaining a strong presence of junctional actin. Scale bar 10µm.

Movie S1: Time course movie of Jeg3 WT, $Ezr^{-/-}Rdx^{-/-}$ and $LOK^{-/-}SLK^{-/-}$ cells treated with 10nM calyculin A over 1 hour.

Movie S2: Time course movie of Jeg3 WT, and $Ezr^{-/-}Rdx^{-/-}$ $LOK^{-/-}SLK^{-/-}$ cells treated with 10nM calyculin A and 25uM blebbistatin over 1 hour. Blebbistatin treatment was added 30 minutes prior to movie start.

Movie S3: Time course movie of $Ezr^{-/-}Rdx^{-/-}$ and $LOK^{-/-}SLK^{-/-}$ cells transfected with phosphomimetic ezrin (Ezrin-T567E) treated with 10nM calyculin A over 1 hour.

CITATIONS

Arber S, Barbayannis FA, Hanser H, Schnelder C, Stanyon CA, Bernards O, Caroni P. 1998. Regulation of actin dynamics through phosphorylation of cofilin by LIM- kinase. *Nature* **393**:805–809. doi:10.1038/31729

Arnold TR, Shawky JH, Stephenson RE, Dinshaw KM, Higashi T, Huq F, Davidson LA, Miller AL. 2019. Anillin regulates epithelial cell mechanics by structuring the medial-apical actomyosin network. *Elife* **8**:39065. doi:10.7554/eLife.39065

Bagci H, Sriskandarajah N, Robert A, Boulais J, Elkholi IE, Tran V, Lin Z-YY, Thibault M-PP, Dubé N, Faubert D, Hipfner DR, Gingras A-CC, Côté J-FF. 2020. Mapping the proximity interaction network of the Rho-family GTPases reveals signalling pathways and regulatory mechanisms. *Nat Cell Biol* **22**:120–134. doi:10.1038/s41556-019-0438-7

Baumgartner M, Sillman AL, Blackwood EM, Srivastava J, Madson N, Schilling JW, Wright JH, Barber DL. 2006. The Nck-interacting kinase phosphorylates ERM proteins for formation of lamellipodium by growth factors. *Proc Natl Acad Sci U S A* **103**:13391–13396. doi:10.1073/pnas.0605950103

Belkina N V., Liu Y, Hao J-JJJ, Karasuyama H, Shaw S. 2009. LOK is a major ERM kinase in resting lymphocytes and regulates cytoskeletal rearrangement through ERM phosphorylation. *Proc Natl Acad Sci U S A* **106**:4707–4712. doi:10.1073/pnas.0805963106

Bretscher A. 1989. Rapid phosphorylation and reorganization of ezrin and spectrin accompany morphological changes induced in A-431 cells by epidermal growth factor. *J Cell Biol* **108**:921–930. doi:10.1083/jcb.108.3.921

Bretscher A, Chambers D, Nguyen R, Reczek D. 2000. ERM-Merlin and EBP50 Protein Families in Plasma Membrane Organization and Function. *Annu Rev Cell Dev Biol* **16**:113–143. doi:10.1146/annurev.cellbio.16.1.113

Chiasson-Mackenzie C, Morris ZS, Liu CH, Bradford WB, Koorman T, McClatchey AI. 2018. Merlin/ERM proteins regulate growth factor-induced macropinocytosis and receptor recycling by organizing the plasma membrane:Cytoskeleton interface. *Genes Dev* **32**:1201–1214. doi:10.1101/gad.317354.118

Clucas J, Valderrama F. 2015. ERM proteins in cancer progression. *J Cell Sci* **128**:1253–1253. doi:10.1242/jcs.170027

Fehon RG, McClatchey AI, Bretscher A. 2010. Organizing the cell cortex: The role of ERM proteins. *Nat Rev Mol Cell Biol* **11**:276–287. doi:10.1038/nrm2866

Fukata Y, Kimura K, Oshiro N, Saya H, Matsuura Y, Kaibuchi K. 1998. Association of the myosin-binding subunit of myosin phosphatase and moesin: Dual regulation of moesin phosphorylation by Rho-associated kinase and myosin phosphatase. *J Cell Biol* **141**:409–418. doi:10.1083/jcb.141.2.409

Garbett D, LaLonde DP, Bretscher A. 2010. The scaffolding protein EBP50 regulates microvillar assembly in a phosphorylation-dependent manner. *J Cell Biol* **191**:397–413. doi:10.1083/jcb.201004115

Gary R, Bretscher A. 1995. Ezrin self-association involves binding of an N-terminal domain to a normally masked C-terminal domain that includes the F-actin binding site. *Mol Biol Cell* **6**:1061–75. doi:10.1091/mbc.E12-02-0152

Gloerich M, Ten Klooster JP, Vliem MJ, Koorman T, Zwartkruis FJ, Clevers H, Bos JL. 2012. Rap2A links intestinal cell polarity to brush border formation. *Nat Cell Biol* **14**:793–801. doi:10.1038/ncb2537

Haas MA, Vickers JC, Dickson TC. 2007. Rho kinase activates ezrin-radixin-moesin (ERM) proteins and mediates their function in cortical neuron growth, morphology and motility in vitro. *J Neurosci Res* **85**:34–46. doi:10.1002/jnr.21102

Hall A. 1998. Rho GTpases and the actin cytoskeleton. *Science (80-)* **279**:509–514. doi:10.1126/science.279.5350.509

Hall A, Nobes CD. 2000. Rho GTPases: Molecular switches that control the organization and dynamics of the actin cytoskeleton. *Philos Trans R Soc B Biol Sci* **355**:965–970. doi:10.1098/rstb.2000.0632
Hanono A, Garbett D, Reczek D, Chambers DN, Bretscher A. 2006. EPI64 regulates microvillar subdomains and structure. *J Cell Biol* **175**:803–813. doi:10.1083/jcb.200604046
Hartsock A, Nelson WJ. 2008. Adherens and tight junctions: Structure, function and connections to the actin cytoskeleton. *Biochim Biophys Acta - Biomembr*. doi:10.1016/j.bbamem.2007.07.012
Hayashi K, Yonemura S, Matsui T, Tsukita S. 1999. Immunofluorescence detection of ezrin/radixin/moesin (ERM) proteins with their carboxyl-terminal threonine phosphorylated in cultured cells and tissues. *J Cell Sci* **112**:1149–1158.
Hebert AM, DuBoff B, Casaletto JB, Gladden AB, McClatchey AI. 2012. Merlin/ERM proteins establish cortical asymmetry and centrosome position. *Genes Dev* **26**:2709–2723. doi:10.1101/gad.194027.112
Hipfner DR, Cohen SM. 2003. The Drosophila sterile-20 kinase slik controls cell proliferation and apoptosis during imaginal disc development. *PLoS Biol* **1**:244–256. doi:10.1371/journal.pbio.0000035
Hipfner DR, Keller N, Cohen SM. 2004. Slik Sterile-20 kinase regulates Moesin activity to promote epithelial integrity during tissue growth. *Genes Dev* **18**:2243–2248. doi:10.1101/gad.303304
Ishihara H, Martin BL, Brautigan DL, Karaki H, Ozaki H, Kato Y, Fusetani N, Watabe S, Hashimoto K, Uemura D, Hartshorne DJ. 1989. Calyculin A and okadaic acid: Inhibitors of protein phosphatase activity. *Biochem Biophys Res Commun* **159**:871–877. doi:10.1016/0006-291X(89)92189-X
Jankovics F, Sinka R, Lukácsovich T, Erdélyi M. 2002. MOESIN crosslinks actin and cell membrane in Drosophila oocytes and is required for OSKAR anchoring. *Curr Biol* **12**:2060–2065. doi:10.1016/S0960-9822(02)01256-3
Kimura K, Ito M, Amano M, Chihara K, Fukata Y, Nakafuku M, Yamamori B, Feng J, Nakano T, Okawa K, Iwamatsu A, Kaibuchi K. 1996. Phosphorylation and activation of myosin by Rho-associated kinase (Rho- kinase). *J Biol Chem* **271**:20246–20249. doi:10.1074/jbc.271.34.20246
Kuramochi S, Moriguchi T, Kuida K, Endo J, Semba K, Nishida E, Karasuyama H. 1997. LOK is a novel mouse STE20-like protein kinase that is expressed predominantly in lymphocytes. *J Biol Chem* **272**:22679–22684. doi:10.1074/jbc.272.36.22679
LaLonde DP, Garbett D, Bretscher A. 2010. A regulated complex of the scaffolding proteins PDZK1 and EBP50 with ezrin contribute to microvillar organization. *Mol Biol Cell* **21**:1519–29. doi:10.1091/mbc.E10-01-0008
Loomis PA, Zheng L, Sekerková G, Changyaleket B, Mugnaini E, Bartles JR. 2003. Espin cross-links cause the elongation of microvillus-type parallel actin bundles in vivo. *J Cell Biol* **163**:1045–1055. doi:10.1083/jcb.200309093
Maekawa H, Neuner A, Rüthnick D, Schiebel E, Pereira G, Kaneko Y. 2017. Polo-like kinase Cdc5 regulates Spc72 recruitment to spindle pole body in the methylotrophic yeast ogataea polymorpha. *Elife* **6**:1–28. doi:10.7554/eLife.24340
Marjoram RJ, Lessey EC, Burridge K. 2014. Regulation of RhoA Activity by Adhesion Molecules and Mechanotransduction. *Curr Mol Med* **14**:199–208. doi:10.2174/1566524014666140128104541
Matsui T, Maeda M, Doi Y, Yonemura S, Amano M, Kaibuchi K, Tsukita Sachiko, Tsukita Shoichiro. 1998. Rho-kinase phosphorylates COOH-terminal threonines of ezrin/radixin/moesin (ERM) proteins and regulates their head-to-tail association. *J Cell Biol* **140**:647–657. doi:10.1083/jcb.140.3.647
Matsui T, Yonemura S, Tsukita SS, Tsukita SS. 1999. Activation of ERM proteins in vivo by Rho

involves phosphatidylinositol 4-phosphate 5-kinase and not ROCK kinases. *Curr Biol* **9**:1259–1262. doi:10.1016/s0960-9822(99)80508-9
McCormack J, Welsh NJ, Braga VMM. 2013. Cycling around cell-cell adhesion with rho GTPase regulators. *J Cell Sci*. doi:10.1242/jcs.097923
Meenderink LM, Gaeta IM, Postema MM, Cencer CS, Chinowsky CR, Krystofiak ES, Millis BA, Tyska MJ. 2019. Actin Dynamics Drive Microvillar Motility and Clustering during Brush Border Assembly. *Dev Cell* **50**:545-556.e4. doi:10.1016/j.devcel.2019.07.008
Neisch AL, Formstecher E, Fehon RG. 2013. Conundrum, an ARHGAP18 orthologue, regulates RhoA and proliferation through interactions with Moesin. *Mol Biol Cell* **24**:1420–1433. doi:10.1091/mbc.E12-11-0800
Ng T, Parsons M, Hughes WE, Monypenny J, Zicha D, Gautreau A, Arpin M, Gschmeissner S, Verveer PJ, Bastiaens PIH, Parker PJ. 2001. Ezrin is a downstream effector of trafficking PKC-integrin complexes involved in the control of cell motility. *EMBO J* **20**:2723–2741. doi:10.1093/emboj/20.11.2723
Oshiro N, Fukata Y, Kaibuchi K. 1998. Phosphorylation of moesin by Rho-associated kinase (Rho-kinase) plays a crucial role in the formation of microvilli-like structures. *J Biol Chem* **273**:34663–34666. doi:10.1074/jbc.273.52.34663
Pakkanen R, Hedman K, Turunen O. 1987. Microvillus-specific M 75,000 plasma membrane protein of human choriocarcinoma cells. *J Histochem Cytochem* **35**:809–816. doi:10.1177/35.8.3298422
Pearson MA, Reczek D, Bretscher A, Karplus PA. 2000. Structure of the ERM protein moesin reveals the FERM domain fold masked by an extended actin binding tail domain. *Cell* **101**:259–270. doi:10.1016/S0092-8674(00)80836-3
Pelaseyed T, Sauvanet C, Viswanatha R, Filter JJ, Goldberg ML, Bretscher A. 2017. Ezrin activation by LOK phosphorylation involves a PIP2-dependent wedge mechanism. *Elife* **6**:1–18. doi:10.7554/eLife.22759
Pietromonaco SF, Simons PC, Altman A, Elias L. 1998. Protein kinase C-θ phosphorylation of moesin in the actin-binding sequence. *J Biol Chem* **273**:7594–7603. doi:10.1074/jbc.273.13.7594
Ratheesh A, Gomez GA, Priya R, Verma S, Kovacs EM, Jiang K, Brown NH, Akhmanova A, Stehbens SJ, Yap AS. 2012. Centralspindlin and alpha-catenin regulate Rho signalling at the epithelial zonula adherens. *Nat Cell Biol* **14**:818–828. doi:10.1038/ncb2532
Reczek D, Berryman M, Bretscher A. 1997. Identification of EPB50: A PDZ-containing phosphoprotein that associates with members of the ezrin-radixin-moesin family. *J Cell Biol* **139**:169–179. doi:10.1083/jcb.139.1.169
Reyes CC, Jin M, Breznau EB, Espino R, Delgado-Gonzalo R, Goryachev AB, Miller AL. 2014. Anillin regulates cell-cell junction integrity by organizing junctional accumulation of Rho-GTP and actomyosin. *Curr Biol* **24**:1263–1270. doi:10.1016/j.cub.2014.04.021
Rodriguez-Boulan E, Macara IG. 2014. Organization and execution of the epithelial polarity programme. *Nat Rev Mol Cell Biol* **15**:225–242. doi:10.1038/nrm3775
Sanjana NE, Shalem O, Zhang F. 2014. Improved vectors and genome-wide libraries for CRISPR screening. *Nat Methods*. doi:10.1038/nmeth.3047
Sanson M, Marineau C, Desmaze C, Lutchman M, Ruttledge M, Baron C, Narod S, Delattre O, Lenoir G, Thomas G, Aurlas A, Rouleau GA. 1993. Germline deletion in a neurofibromatosis type 2 kindred inactivates the NF2 gene and a candidate meningioma locus. *Hum Mol Genet* **2**:1215–1220. doi:10.1093/hmg/2.8.1215
Saotome I, Curto M, McClatchey AI. 2004. Ezrin is essential for epithelial organization and villus morphogenesis in the developing intestine. *Dev Cell* **6**:855–864. doi:10.1016/j.devcel.2004.05.007
Sauvanet C, Garbett D, Bretscher A. 2015. The function and dynamics of the apical scaffolding protein E3KARP are regulated by cell-cycle phosphorylation. *Mol Biol Cell* **26**:3615–3627.

doi:10.1091/mbc.E15-07-0498
Shalem O, Sanjana NE, Hartenian E, Shi X, Scott DA, Mikkelsen TS, Heckl D, Ebert BL, Root DE, Doench JG, Zhang F. 2014. Genome-scale CRISPR-Cas9 knockout screening in human cells. *Science (80-)* **343**:84–87. doi:10.1126/science.1247005
Speck O, Hughes SC, Noren NK, Kulikauskas RM, Fehon RG. 2003. Moesin functions antagonistically to the Rho pathway to maintain epithelial integrity. *Nature* **421**:83–87. doi:10.1038/nature01295
ten Klooster JP, Jansen M, Yuan J, Oorschot V, Begthel H, Di Giacomo V, Colland F, de Koning J, Maurice MM, Hornbeck P, Clevers H. 2009. Mst4 and Ezrin Induce Brush Borders Downstream of the Lkb1/Strad/Mo25 Polarization Complex. *Dev Cell* **16**:551–562. doi:10.1016/j.devcel.2009.01.016
Terry SJ, Zihni C, Elbediwy A, Vitiello E, San IVLC, Balda MS, Matter K. 2011. Spatially restricted activation of RhoA signalling at epithelial junctions by p114RhoGEF drives junction formation and morphogenesis. *Nat Cell Biol* **13**:159–166. doi:10.1038/ncb2156
Tran Quang C. 2000. Ezrin function is required for ROCK-mediated fibroblast transformation by the Net and Dbl oncogenes. *EMBO J* **19**:4565–4576. doi:10.1093/emboj/19.17.4565
Trofatter JA, MacCollin MM, Rutter JL, Murrell JR, Duyao MP, Parry DM, Eldridge R, Kley N, Menon AG, Pulaski K, Haase VH, Ambrose CM, Munroe D, Bove C, Haines JL, Martuza RL, MacDonald ME, Seizinger BR, Short MP, Buckler AJ, Gusella JF. 1993. A novel moesin-, ezrin-, radixin-like gene is a candidate for the neurofibromatosis 2 tumor suppressor. *Cell* **72**:791–800. doi:10.1016/0092-8674(93)90406-G
Turunen O, Wahlström T, Vaheri A. 1994. Ezrin has a COOH-terminal actin-binding site that is conserved in the ezrin protein family. *J Cell Biol* **126**:1445–1453. doi:10.1083/jcb.126.6.1445
Velasco G, Armstrong C, Morrice N, Frame S, Cohen P. 2002. Phosphorylation of the regulatory subunit of smooth muscle protein phosphatase 1M at Thr850 induces its dissociation from myosin. *FEBS Lett* **527**:101–104. doi:10.1016/S0014-5793(02)03175-7
Viswanatha R, Ohouo PY, Smolka MB, Bretscher A. 2012. Local phosphocycling mediated by LOK/SLK restricts ezrin function to the apical aspect of epithelial cells. *J Cell Biol* **199**:969–984. doi:10.1083/jcb.201207047
Yang N, Higuchi O, Ohashi K, Nagata K, Wada A, Kangawa K, Nishida E, Mizuno K. 1998. Cofilin phosphorylation by LIM-kinase 1 and its role in Rac-mediated actin reorganization. *Nature* **393**:809–812. doi:10.1038/31735
Zihni C, Balda MS, Matter K. 2014. Signalling at tight junctions during epithelial differentiation and microbial pathogenesis. *J Cell Sci* **127**:3401–3413. doi:10.1242/jcs.145029